Pressure Ridge Ice Scour Experiment
PRISE Phase 3C : Extreme Ice Scour Event - Modeling and Interpretation
Milestone 2: Centrifuge Test
PRSA02 Data Report

Contract Report

Prepared for

BP Alaska
Chevron Petroleum Technology
Exxon Production Research Company
Petro-Canada
Union Texas Petroleum

Prepared by

C-CORE

C-CORE Publication 97-C6
April, 1997

The correct citation for this report is :

Winsor, R., and Parsons, G. (1997). " Pressure Ridge Ice Scour Experiment Phase 3c, Extreme Ice Scour Event - Modeling and Interpretation, Milestone 2 : Centrifuge Test PRSA02 Data Report ". Contract Report for BP Alaska, Chevron Petroleum Technology, Exxon Production Research Company, Petro-Canada, and Union Texas Petroleum, C-CORE Publication 97-C6.

QUALITY CONTROL REPORT

Clients:	BP Alaska, Chevron Petroleum Technology, Exxon Production Research Company, Petro-Canada, and Union Texas Petroleum
Project:	Pressure Ridge Ice Scour Experiment-PRISE Phase 3c Extreme Ice Scour Event - Centrifuge Modeling and Interpretation
Client's Contract Ref.:	-
C-CORE Cost Center:	340388

Document Title:	Pressure Ridge Ice Scour Experiment (PRISE Phase 3c) Extreme Ice Scour Event - Modeling and Interpretation Milestone 2 : Centrifuge Test PRSA02 Data Report
C-CORE Pub. No.:	97-C6
Prepared By:	Rod Winsor, George Parsons
Date:	February, 1997

Reviewers	Document Accepted Date	Signature
Technical Accuracy	15 April 97	S Hurley
	15 April 97	D Nikl
	5-4-97	R. P
Syntax		
Layout & Presentation		
General Evaluation	5-4-97	R. P

Approval for Release

Date: April 15/97

for President & CEO

TABLE OF CONTENTS

1. INTRODUCTION

Centrifuge Test PRSA02 was designed to investigate the forces and soil deformation effects of an extreme full-scale ice scouring event in a medium dense uniform sand through the application of centrifuge modelling. Model preparation began on January 15, 1997. The test was performed on January 30, 1997 and post test investigations of subsurface soil deformation were carried out immediately after the test.

As a result of the limited capacity of the horizontal drive, the scour could not be conducted at 150 g (1:150 scale). After repeated attempts at lowering the g-level the scour was successful at 75 g, 75 gravities at the base of the model keel. The attack angle of the model keel was set at 15 degrees to the horizontal. The keel width was 100 mm and the proposed scour cut depth was 33 mm, corresponding to a prototype scour with nominal dimensions of 7.5 m width and 2.5 m depth. The actual scoured surface profile was assessed following completion of the centrifuge test. The specified rate of advance of the model keel was 100 mm/s. The model scouring was conducted in a testbed of saturated reconstituted soil which comprised 100% F-110 Silica sand.

2. PROGRAM SUMMARY

Table 1 presents an updated summary of the test schedule.

Table 1 Updated PRISE Phase 3c Test Schedule

Test Designation	Testbed Material	Scour Depth (m)	Attack Angle (deg)	Test Status / Completion Date
PROOF	Medium Dense Sand	5.0	30	Completed/June 1996
PRCS01	Medium Stiff Silty Clay	5.0	30	Completed/July 1996
TRIAL(PRS01)	Pure Silt	0.5	30	Completed/Aug. 1996
PRSC01	Clayey Silt	1.0	15	Completed/Oct. 1996
PRSC02	Clayey Silt	2.0	15	Completed/Nov. 1996
PRCS02	Medium Stiff Silty Clay	5.0	15	Completed/Dec.1996
PRSA01	Medium Dense Sand	5.0	30	Completed/Jan. 1997
PRSA02	Medium Dense Sand	2.5	15	This Report 1997
PRSA03	Medium Dense Sand	2.0	15	Proposed/Feb. 1997
PRSA04	Medium Dense Sand	2.0	15	Proposed/Feb. 1997

3. MODEL SEABED PREPARATION

The model seabed was prepared from fine sand with the index properties listed in Table 2. The sand was dry pluviated into the centrifuge strongbox from a large hopper on a bed of dense coarse base drainage sand in lifts of approximately 15 mm in thickness. The mass flow rate of sand was controlled by a flow control valve plate at the hopper base release orifice. The dry density (ρ_d) of the sand was periodically monitored during placement using small density cups (Table 3). The average dry density and relative density (D_r) were approximately 1.66 g/cc and 73.0 %, respectively.

After each lift was placed, it was levelled to the appropriate predetermined elevation using a vacuum system and a thin veneer of blue colored sand was placed on the surface. Once this veneer of colored sand was placed, lines of lead shot were partially and evenly embedded into the colored material. Both the colored sand layers and the lead shot grids were specifically designed and applied to provide first hand visual and radiographic data on subsurface scour deformations. Pore pressure transducers (PPT's) were also installed in the testbed at strategic predetermined elevations to monitor the pore fluid pressures developed during the centrifuge model test. Complete details on the layout and placement of the colored sand layers, lead shot grids and PPT's are presented in Figure 1.

Upon completion of testbed, it was gradually saturated from the base upwards, under a vacuum of approximately 70 kPa. This procedure was employed to ensure complete saturation of the sand specimen with negligible disturbance. After the saturation procedure was complete equally spaced lines of colored spaghetti marker strands were inserted to a depth of approximately 170 mm into the testbed as shown in Figure 4. These markers were specifically placed so that they could be excavated after the model scour event to provide quantitative data on the lateral horizontal displacement field developed off the scour centerline with passage of the keel.

Table 2 Properties of F-110 Silica Sand

Maximum dry density	$\rho_{dmax} = 1.78$ g/cc
Minimum dry density	$\rho_{dmin} = 1.41$ g/cc
Specific gravity	$Gs = 2.66$
Effective grain size	$D_{10} = 0.10$
Mean grain size	$D_{50} = 0.14$
Uniformity coefficient	$Cu = 1.50$

Table 3 Sand state at placement

Approximate depth below testbed surface (mm)	ρ_d (g/cc)	D_R (%)
0 - 40	1.67	74.2
40 - 80	1.67	74.2
80 - 120	1.67	74.9
120 - 160	1.65	70.2
160 - 200	1.66	73.2
200 - 240	1.66	72.5

4. INSTRUMENTATION AND DATA ACQUISITION

Details of PRISE Phase 3c experimental devices and procedures were presented in the Centrifuge Proof Test Progress Report (C-CORE Publication 96-C21). Table 4 provides a summary of the instrumentation used in Test PRSA02. In total, 20 active transducers were employed, including instrumentation used to measure the vertical and horizontal loads and contact pressures acting on the model keel, the keel position during the event, as well as the pore water pressure changes induced within the sand testbed. Figure 2 shows the locations of the transducers which were attached to the model keel, and Table 5 indicates the testbed positions of the individual pore pressure transducers. Locations in the model are described with reference to a right-handed coordinate system with origin at the centerline of the strongbox; the y-axis is directed along the center axis of the scour and defines the horizontal position of the model keel in relation to the strongbox wall at the initial keel position; the z-axis is directed laterally outward from the scour axis, and the x-axis is vertical with positive values measured as depths below the initial sand surface, established following settlement.

Table 4 Test Instrumentation

Device	Identification	Measured or Derived Quantity
Tension Cell	TC04A	model horizontal force
Tension Cell	TC04B	model horizontal force
Load Cell	LC09	model vertical force / keel front
Load Cell	LC02	model vertical force / keel front
Load Cell	LC03	model vertical force / keel rear
Load Cell	LC06	model vertical force / keel rear
Pressure Transducer	PT08	contact pressure / horizontal base
Pressure Transducer	PT11	contact pressure / inclined surface
Pressure Transducer	PT09	contact pressure / inclined surface
Pressure Transducer	PT504863	contact pressure / inclined surface
String Potentiometer	SP02	model horizontal position
Displacement Transducer	LDT12	sand surface settlement
Pore Pressure Transducer	PPT6925	soil pore water pressure
Pore Pressure Transducer	PPT7474	soil pore water pressure
Pore Pressure Transducer	PPT7476	soil pore water pressure
Pore Pressure Transducer	PPT7478	soil pore water pressure
Pore Pressure Transducer	PPT4378	surface water level
Pore Pressure Transducer	PPT8063	standpipe water level
CPT Load Cell	SANDCONE #2	cone tip resistance
CPT Vert. Potentiometer	VDISPL	cone vertical displacement

Table 5. Pore Pressure Transducer Locations

Transducer	X (mm)	Y (mm)	Z (mm)	Comments
PPT7474	46	415	0	beneath testbed surface at centerline
PPT7478	81	415	0	beneath testbed surface at centerline
PPT6925	155	415	0	beneath testbed surface at centerline
PPT7476	204	415	0	beneath testbed surface at centerline

5. CENTRIFUGE SWING - UP AND SETTLEMENT

To begin the settlement phase of the test, the centrifuge was accelerated to 80 rpm over a time duration of approximately 10 minutes. This speed equated to 75 gravities at the base of the model keel. At this acceleration level, the model keel represented a prototype width of 7.5 m and a prototype scour depth of 75 times the model cut depth.

Due to the limited capacity of the horizontal drive the package had to be swung-up a total of six times. A linear displacement transducer (LDT) was employed to measure surface settlement. The apparent total sand surface settlement was approximately 7.0 mm. The LDT response for the sixth swing-up is presented in Figure 3. Based on this figure and the LDT responses for the previous swing ups which include system compliance, it was estimated that the total surface settlement was 7.0 mm yielding a dry density and relative density at the time of scour of approximately 1.74 g/cc and 90.0%, respectively.

6. IN - FLIGHT CONE PENETRATION TESTING

The C-CORE cone penetration test (CPT) apparatus was added to the test package equipment to allow for the estimation of soil properties based on the results of cone penetration tests carried out under the state of stresses actually experienced during centrifuge rotation. The cone tip employed had an angle of 60 degrees with a cross-sectional area of 100 mm^2. The support structure for the apparatus was modified to accommodate the revised test configuration used in the Phase 3C experimental programme.

A cone penetration test was performed at the location shown in Figure 4, adopting a nominal rate of penetration equal to 3 mm/s. The test was conducted subsequent to the establishment of settlement equilibrium conditions and immediately preceding initiation of the model scouring event. The test record is presented in Figure 5 which displays the profile of cone tip resistance q_c over a total depth of penetration of approximately 180 mm. This profile suggests slightly more resistance than observed in previous PRISE tests, which is reasonable due to the increased sand density. Values of

the effective interpreted cone tip resistance, q_c', for all PRISE tests conducted to date are presented in Table 6 and are calculated using the following relationship,

$$q_c' = q_c - u_0$$

where u_0 is the initial pore pressure at the base of the keel. Plots of q_c / depth often show a bilinear relationship, with the response to about 4 or 5 cone diameters having a milder slope than the response at greater depths. The CPT response near the surface underestimates the strength characteristics of the soil due to interactions with the testbed surface. For this reason, values of q_c in Table 6 were determined by linearly interpolating the CPT response at depth back to shallower depths.

7. MODEL SCOURING EVENT

The model conditions applicable to Test PRSA02 may be summarized as follows:

Model Scale	75 : 1
Scour Width	100 mm
Scour Cut Depth	31.7 mm (target 33.3 mm)
Attack Angle	30 degrees
Velocity	0.1 m/s
Material	Fine uniform sand (D_R = 90 %)

Data acquired during the scouring event included pore pressure measurements and resultant forces and contact pressures acting on the model keel. The total horizontal force was computed through summation of contributions from individual tension load cells (TC04A and TC04B) located at the connection between the drive system pulling cables and the model keel. Figure 6 shows the measured horizontal force for each tension cell plotted against keel displacement during the event. The total average horizontal force imposed under apparent steady state scouring conditions was 4.38 kN at the model scale.

The total vertical force was evaluated through summation of the responses of the four tension/compression load cells (LC02, LC03, LC06, and LC09) which linked the model keel to the carriage assembly. Figure 7 shows the measured vertical force for each load cell, plotted against keel displacement during the event. The response of LC09 was problematic and for this reason no response data are available for the instrument. Since previous results have shown that the responses of load cells at the front or rear of the keel are similar, it was assumed that the response of LC09 was similar to that of LC06. The average steady state values recorded at the front and rear of the model keel were -1.31 and -3.77 kN (-compression, +tension) respectively, at the model scale. The total

average vertical force was -5.09 kN, which implied a vertical / horizontal force ratio of 1.16 for steady state conditions.

The contact pressures developed during the scouring event are displayed in Figure 8 which presents the data records for four interface pressure transducers (PT11, PT09, PT08 and PT504863) mounted on the model keel. The pressure record for the transducer located at the horizontal base of the keel indicated an average response over the duration of the event of approximately 49 kPa. The two pressure transducers situated on the lower positions of the inclined faces of the keel displayed similar average responses of approximately 559 and 555 kPa. The transducer located on the upper position of the inclined face exhibited a slightly lower response of 442 kPa.

Figure 9 shows the keel displacement plotted versus time during the model scouring event, as determined from measurements of the string potentiometer (SP02) which was attached to the carriage assembly. This data record was used to evaluate the horizontal position of the model keel in presentation of the results for each of the other transducers. The actual keel velocity or scour rate was 105.6 mm/s, equal to the slope of the steady state portion of the displacement-time curve.

Pore water pressure changes were recorded by four pore pressure transducers (PPT7474, PPT7478, PPT7476 and PPT6925). The locations of these transducers are shown in Figure 1 and Table 5. The response of PPT 7474 was problematic and for this reason no data are available for the response of this instrument. A summary of the measured excess pore pressure responses during the model scour event is presented in Figure 10. The maximum decrease in pore pressure was approximately 18 kPa for the transducer located closest to the keel. The responses of the other transducers were seen to decrease from 7 to 4 kPa with increasing distance from the keel.

8. INVESTIGATION OF SOIL DEFORMATION

Post-test investigation of the sand testbed included photographic documentation and visual inspection of scour morphology, profiling of the scoured surface, and examination of sub-scour effects through excavation, photography and radiography. Photographs which display two different views of the model scour are presented in Figure 11. The sidewalls of the incision were characterized by a sharply sloping berm of heaved material along the entire length of the scour rising to a maximum elevation on the order of 15 mm above the initial testbed elevation. A substantial frontal spoil mound was developed at the front of the keel, which rose to approximately 30 mm above the initial testbed surface.

Profiles of the deformed sand surface were acquired using the C-CORE laser profiling system. Figure 12 shows an axial section profile measured at the centerline of the model scour. Cross-sectional profiles obtained at horizontal intervals of 50 mm along the scour length are presented in Figures 13 through 23, beginning from y-coordinate equal to 50 mm at the initial position of the model keel. From Figure 12, it is apparent that the average scour depth attained for the steady-state scouring condition was approximately 31.7 mm or 2.4 m at prototype scale. The profile also displays the post-test surface configuration including soil movements (heave) which developed subsequent to passage of the keel. The corresponding berm elevations averaged 15 mm

above the initial surface level or 1.1 m at prototype scale. These values were not determined solely from the laser profiles but were also measured after the package was unloaded. For this test, the laser profiler malfunctioned and hence did not give accurate profiles. The profiles are included in this report to give an overall appreciation for the profile trends along the scour path.

The sand testbed was cut along sections both parallel and perpendicular to the scour axis in order to allow for photographic and radiographic examination of the deformed configuration of the internal colored layers and lead shot (passive marker) grids. Figures 24 and 25 present digitized traces of radiographs which depict sectional views of the lateral and axial grids, respectively. Figures 27-30 present photos of axial testbed sections with colored sand layers and lateral colored spaghetti markers directly beneath the keel at its final position ($y \cong 700$ to 1010) at different lateral distances ($z \cong 0$, 25, 50 and 75 mm) from the centerline of the scour. Figure 31 presents a photo of the lateral testbed section and colored sand layers directly beneath the scour path with coordinates $y \cong 540$ and $z \cong -150$ to 150.

A summary of the test PRSA02 sub-scour displacement records is presented in Figure 26, where representative average centerline values of the horizontal components are plotted against depth below the base of the scour. For this test no measurable vertical displacements were detected. The horizontal displacements shown in this plot were evaluated as the difference between the initial (pre-scour) and final (post scour) axial grid marker positions. In Figure 26, the data point shown at the base of scour is an extrapolated value. All other data points are measured values. This extrapolation is more reliable for the horizontal displacements than for vertical displacements as the radiographic markers in the axial section indicate both the magnitude and the gradient of the horizontal displacements. In cross section, the radiographic markers only indicate the magnitude of the vertical displacement. In Figure 26, horizontal displacements are plotted against final (post-scour) elevation of the radiographic marker.

The maximum value of horizontal displacement at the level of the scour base was 0.6 m at the prototype scale, as indicated from grid measurements acquired at sub-scour positions. The limiting depth below the base of the scour at which significant horizontal displacements were measured was 3.7 m at the prototype scale. Based on these observations horizontal displacements extended to a normalized value on the order of 1.5 scour depths beneath the scour base.

In all of the above estimates of subscour displacement, distortions inherent in the radiograph process have been removed as discussed in C-CORE Publication 96-C34.

9. COMPARATIVE EVALUATION OF TEST RESULTS

The findings of the initial series of PRISE centrifuge model tests were summarized in C-CORE Publication 95-C12. Table 6 presents a comparison of the Test PRSA02 resultant force data with values acquired for all PRISE tests conducted in F-110 Silica sand over a range of relative densities.

The prototype horizontal and vertical components of the scour force derived for steady-state conditions were 24.6 and 28.6 MN respectively in Test PRSA02, which are approximately two to

three times higher than those for other PRISE sand tests conducted at 75g. These force magnitudes are dissimilar, giving rise to a force ratio of 1.16 which is reasonably consistent with most other PRISE sand tests.

The region of large sub-scour soil displacement may be defined approximately for individual scouring events by specification of the apparent maximum values immediately below the scour base (interpolated from the available displacement data) together with the limiting depth, below which measured displacement magnitudes were less than a nominal lower bound of 0.2 m at the corresponding prototype scale. A summary of the results for PRISE tests conducted in F-110 Silica Sand and Test PRSA02 is presented in Table 7 which suggests that the displacement data for Test PRSA02 is reasonable in relation to previous tests.

Table 6 **Prototype Force Data Tabulated for PRISE (F-110 Silica) Sand Tests** (Source Table 5.3 C-CORE Publication 95-C12)

Test	PRSA02	PRSA01	PRISE 01B Drive 2	PRISE 01C Drive 1	PRISE 01C Drive 2	PRISE 09 Drive 1	PRISE 09 Drive 2	PRISE 10 Drive 1	PRISE 10 Drive 2
g-Level	75	150	150	75	75	150	150	150	150
Sand State (D_R) %	90.0	81.0	37.4	37.0	37.0	> 47.2	> 47.2	65.9	65.9
Attack Angle (deg.)	15	30	15	30	15	15	15	30	15
Scour Depth (m)	2.4	4.5	1.69	0.98	1.1	1.18	2.14	1.19	1.16
Scour Width (m)	7.5	15	15	15	15	15	15	30	30
q_c' (kPa) at Keel Base	2223	3349	716	521	559	1435	1925	726	726
Horizontal Force (MN)	24.6	93.8	33.7	8.9	12.2	19.3	40.3	40.5	45.9
Vertical Force (MN)	28.6	123.3	35.1	8.4	14.2	16.4	38.5	38.0	49.9
Force Ratio F_V/F_H	1.16	1.31	1.04	0.94	1.17	0.85	0.95	0.94	1.04

Table 7 **Prototype Centerline Displacement Magnitudes at Scour Base and Limiting Depths below Scour Base - Summary of Results for PRISE Tests in (F-110 Silica) Sand** (Source Figures 89 and 94, Tables 6.7 and 6.8, C-CORE Publication 95-C12)

Test Designation	Horizontal component of sub-scour displacement		Vertical component of sub-scour displacement	
	magnitude at scour base (m)	limiting depth below base (m)	magnitude at scour base (m)	limiting depth below base (m)
PRSA02	0.6	1.6	0	0
PRSA01	2.0	4.6	0.4	1.5
PRISE 01B, Drive 2	2.40	3.45	0.80	4.00
PRISE 01C, Drive 1	0.75	1.95	> 0.23	0.65
PRISE 01C, Drive 2	0.71	3.90	0.19	NA
PRISE 09, Drive 1	3.50	4.40	0.59	2.70
PRISE 09, Drive 2	> 2.40	> 3.75	NA	NA
PRISE 10, Drive 1	0.00	0.00	0.00	0.00
PRISE 10, Drive 2	0.00	0.00	0.00	0.00

10. REFERENCES

Collins, M., Lach, P.R., and Parsons, G. (1996). " Pressure Ridge Ice Scour Experiment Phase 3c, Extreme Ice Scour Event - Modeling and Interpretation, Milestone 1 : Centrifuge Proof Test Progress Report ". Contract report for BP Alaska, Chevron Petroleum Technology, Petro-Canada, and Union Texas Petroleum, C-CORE Publication 96-C21.

Clark et al. (1995). " Pressure Ridge Ice Scour Experiment Phase 3 : Centrifuge Modeling of Ice Keel Scour : Final Report ". Contract report for ARCO Alaska, Chevron Petroleum Technology, Exxon Production Research, Minerals Management Service, Mobil Oil Canada Properties, National Energy Board (Canada), Natural Sciences and Engineering Research Council (Canada), and Petro-Canada Resources, C-CORE Publication 95-C12.

Winsor, R., and O'Neil, P. (1996). " Pressure Ridge Ice Scour Experiment Phase 3c, Extreme Ice Scour Event - Modelling and Interpretation, Milestone 2 : Centrifuge Test PRSC02 Data Report ". Contract report for BP Alaska, Chevron Petroleum Technology, Petro-Canada, and Union Texas Petroleum, C-CORE Publication 96-C34.

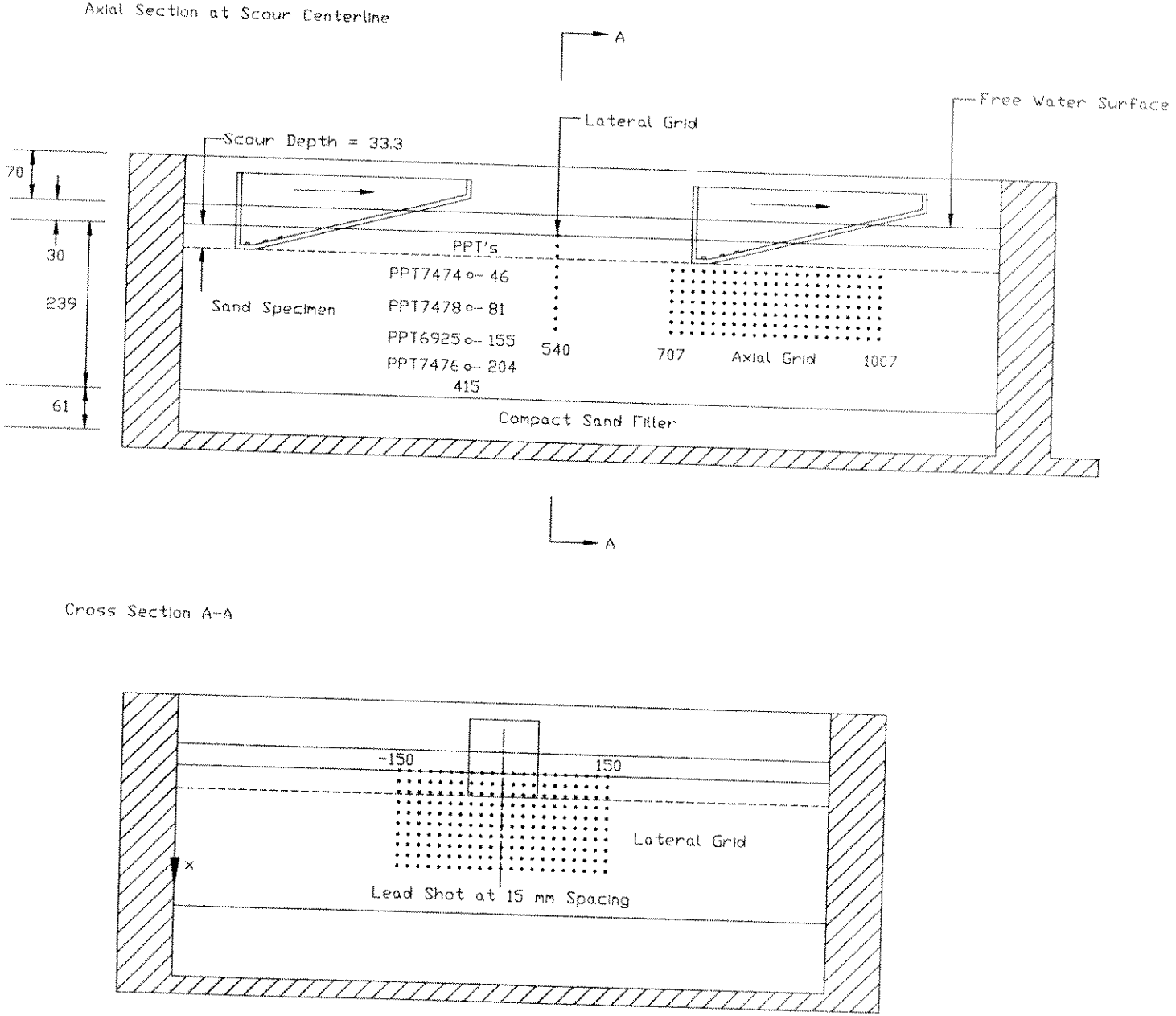

Schematic of Sand Testbed Showing Layout of Instrumentation and Passive Markers (all dimensions in mm)

Fig. No. 1

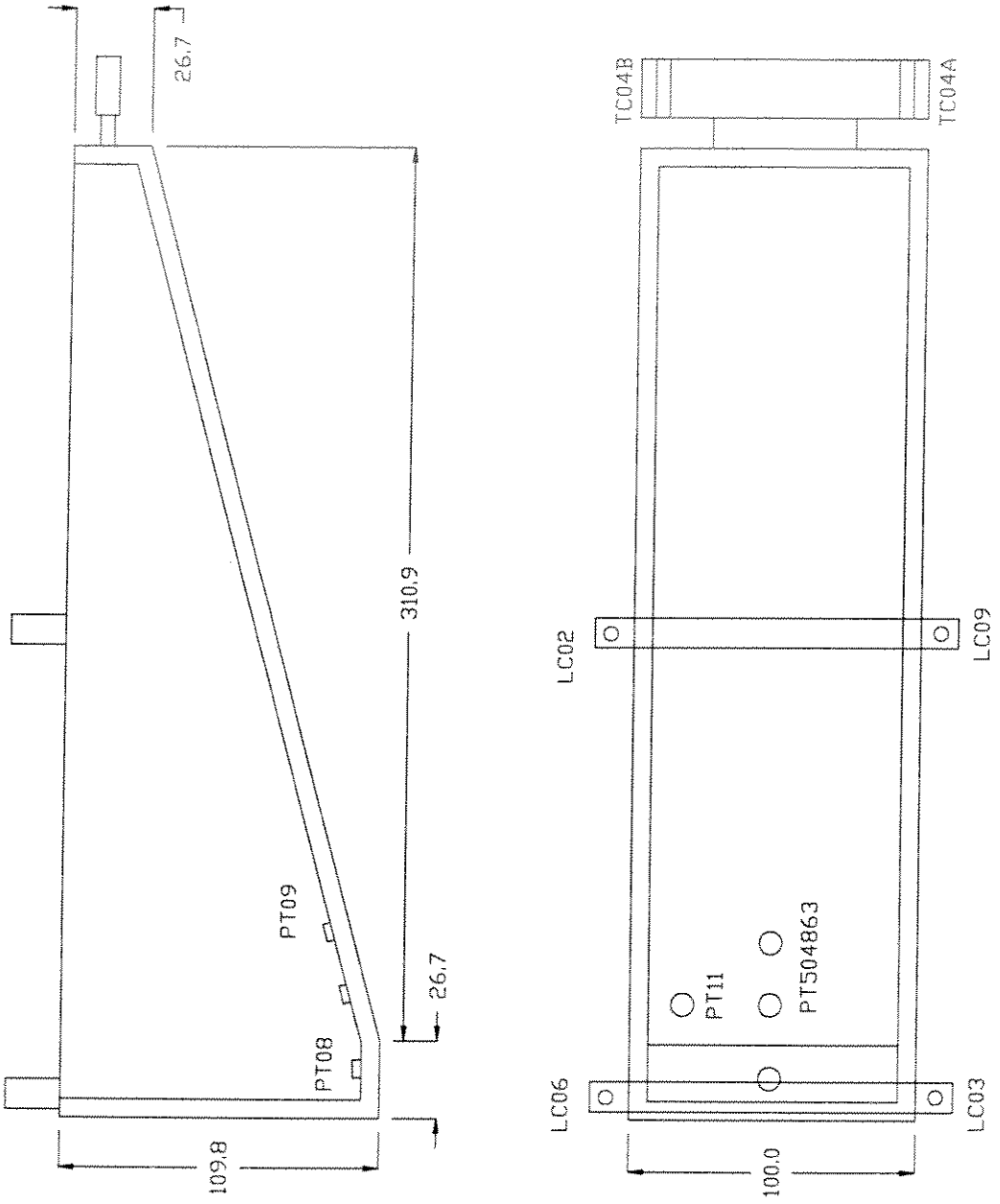

C-CORE

Plan and Side View of Instrumented Model Keel Showing Transducer Locations (all dimensions in mm)

Fig. No. 2

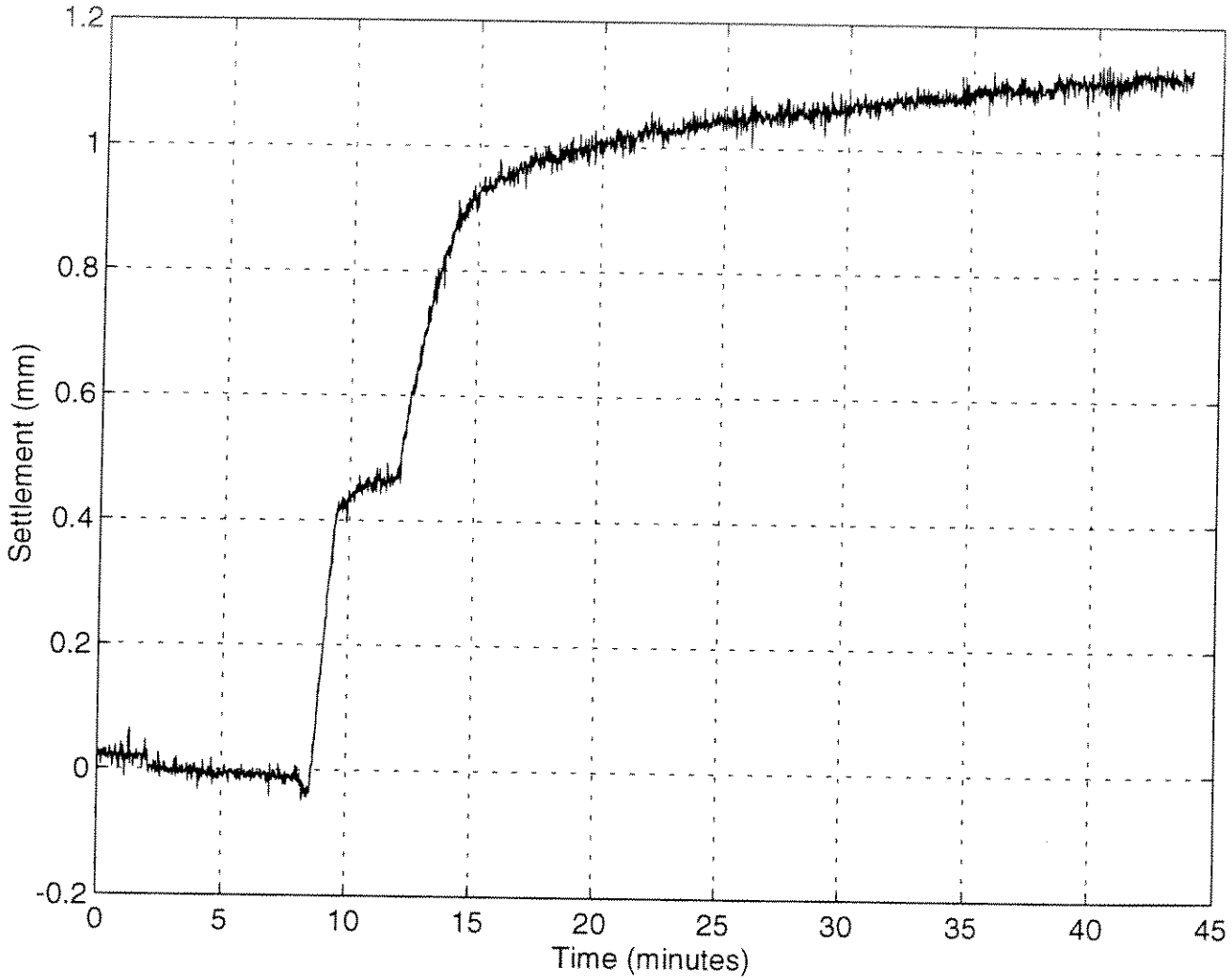

C-CORE

Sand Settlement during Swing Up

Fig. No.

3

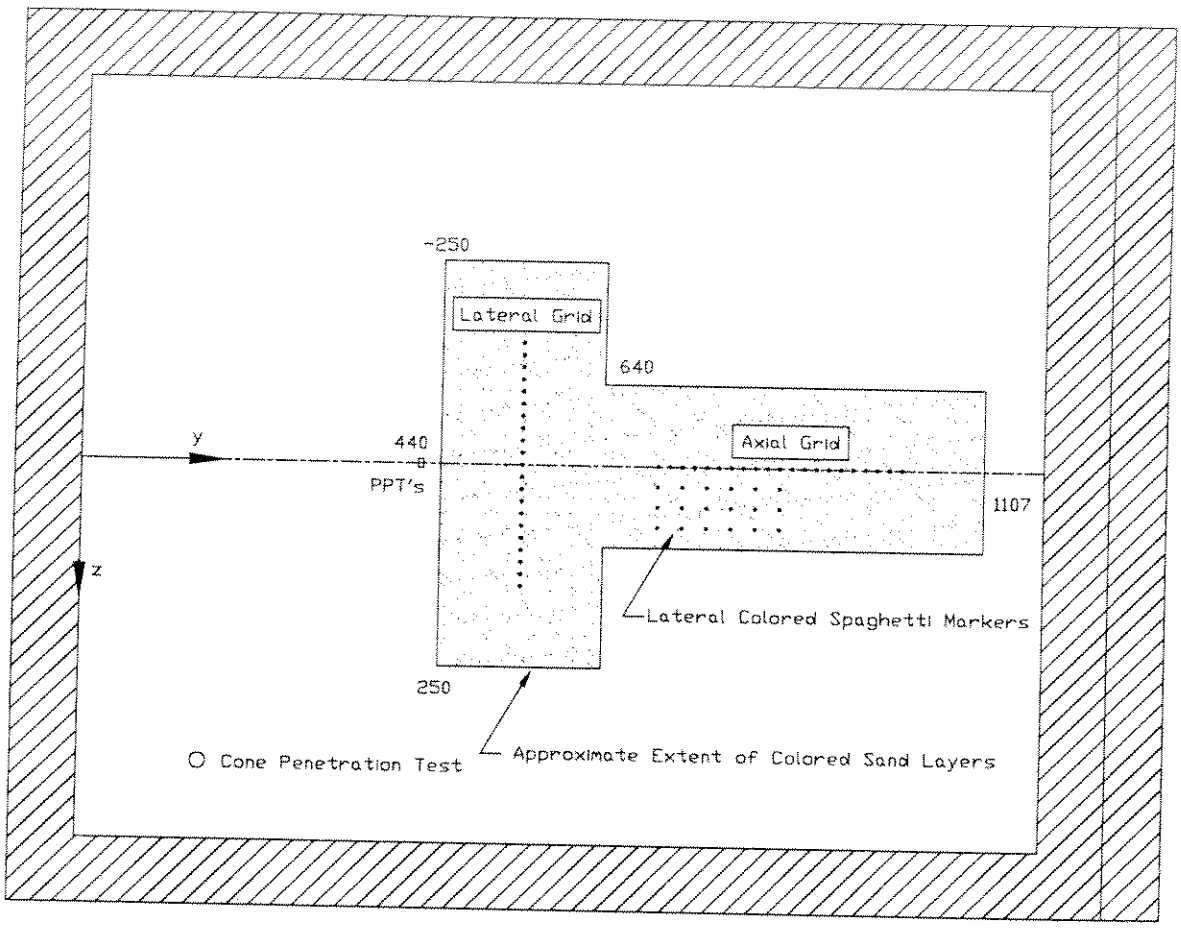

C-CORE

Location of Cone Penetration Test (all dimensions in mm)

Fig. No. 4

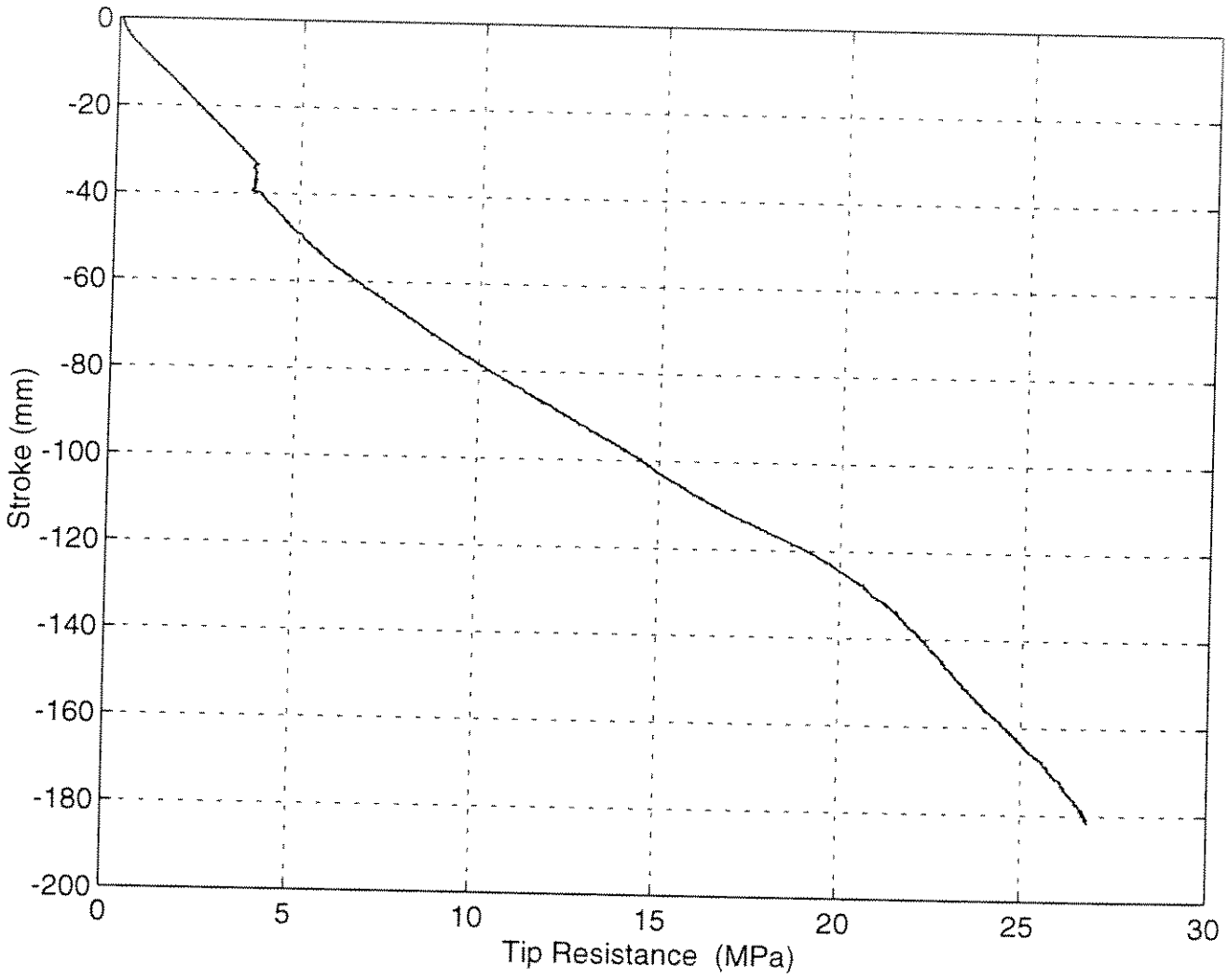

C-CORE

In-Flight Cone Penetration Test Profile

Fig. No.

5

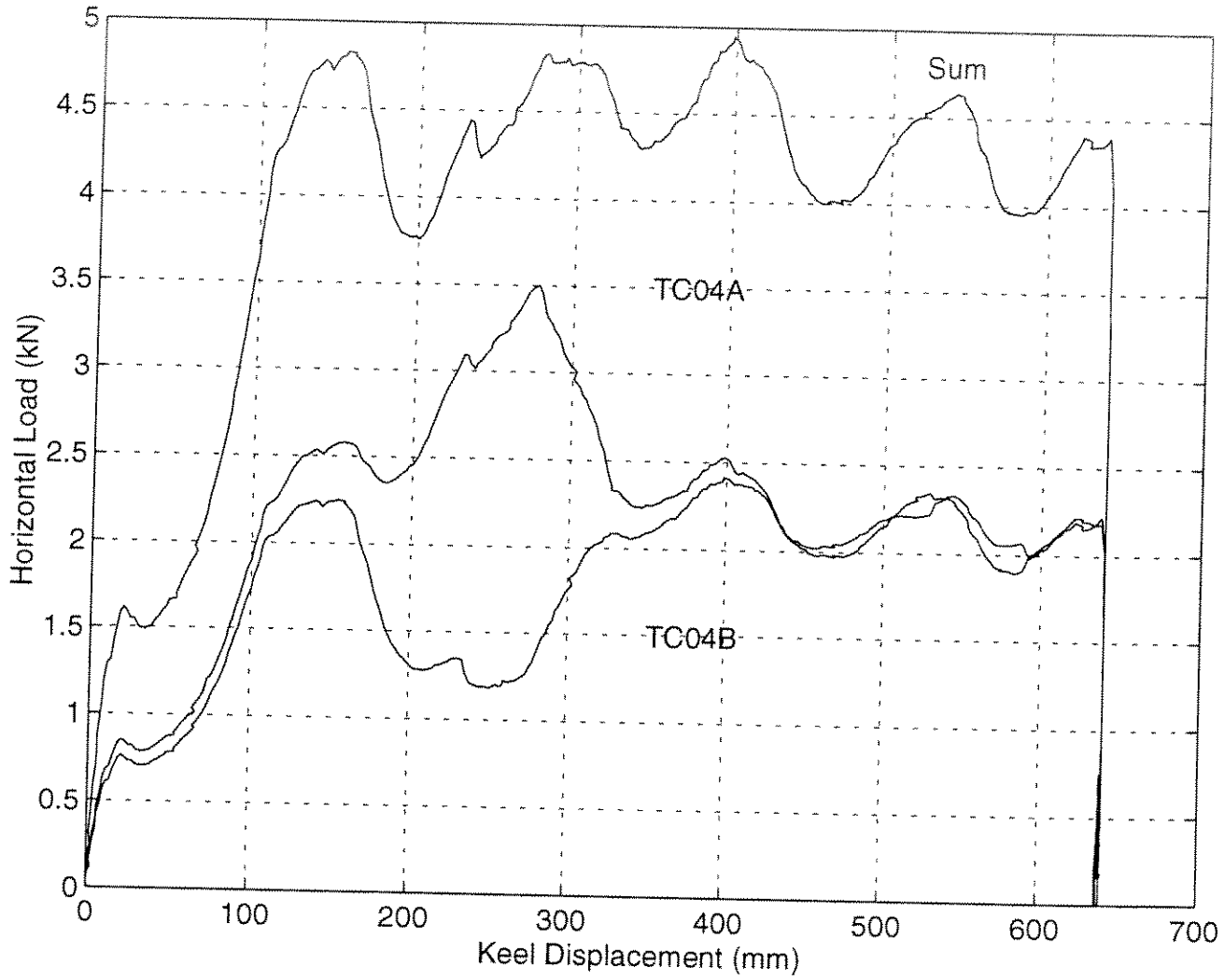

C-CORE

Horizontal Force vs. Displacement for each Tension Cell

Fig. No. 6

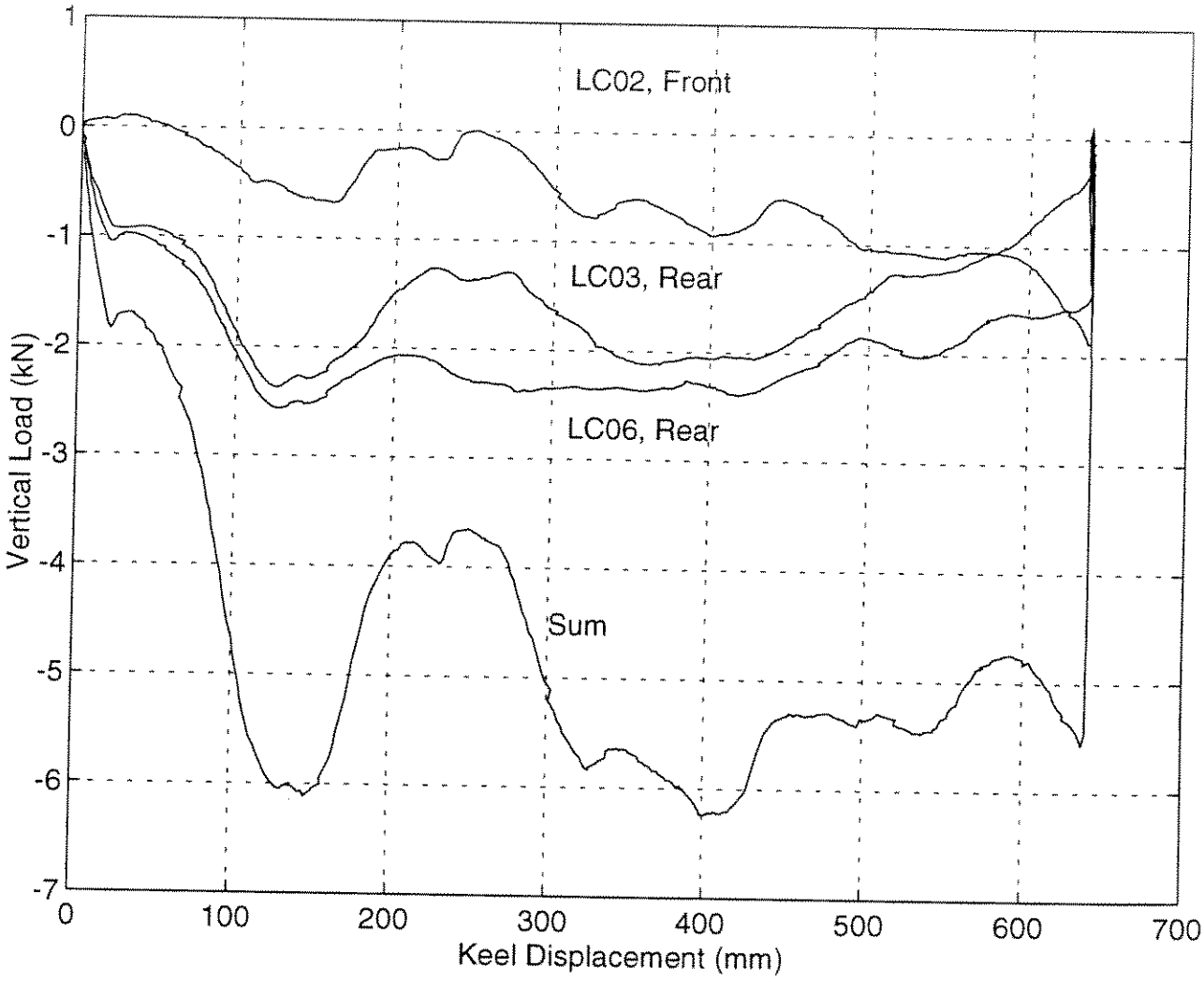

C-CORE

Vertical Force vs. Displacement for each Load Cell

Fig. No. 7

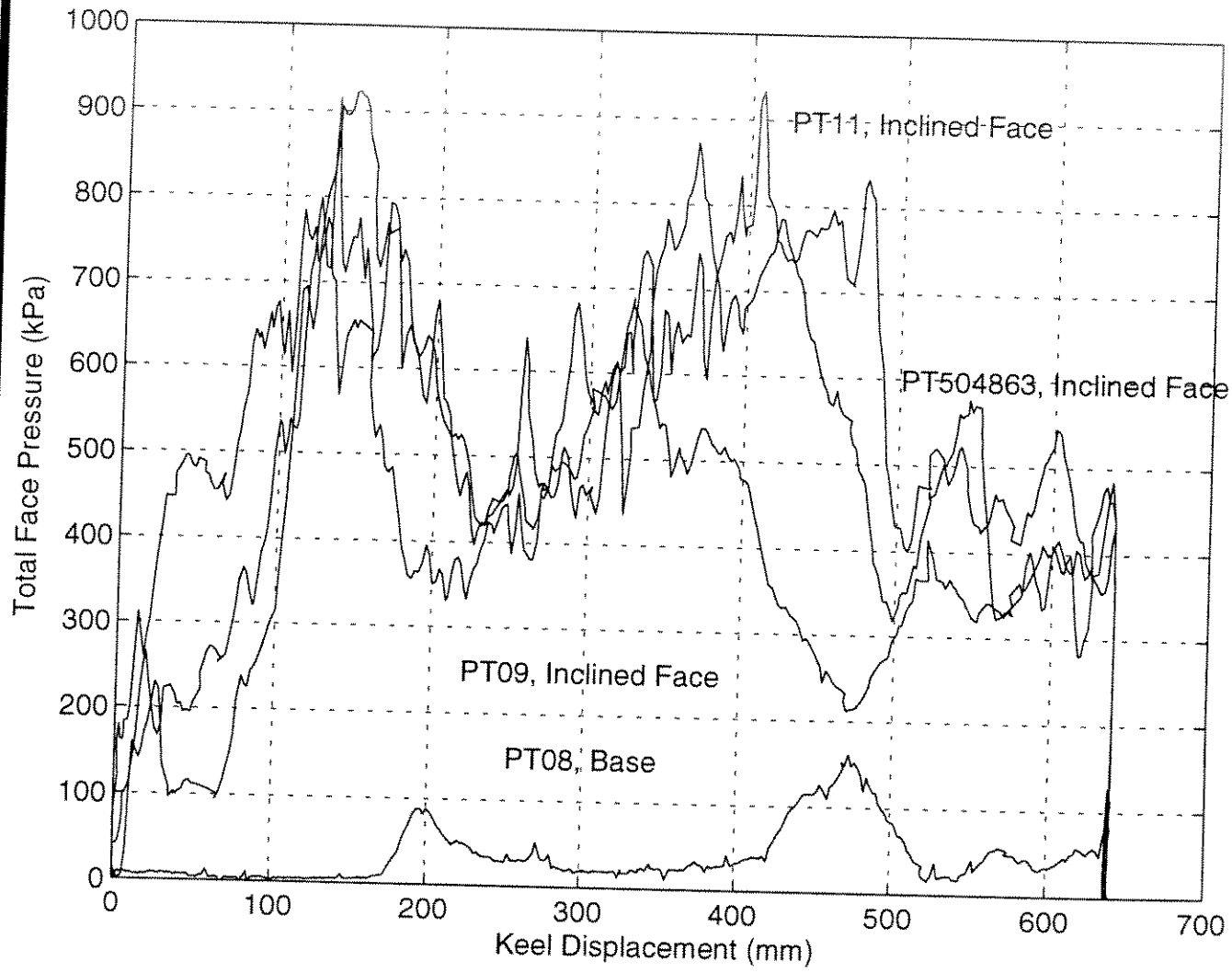

C-CORE

Contact Pressure vs. Displacement for each Pressure Transducer

Fig. No.

8

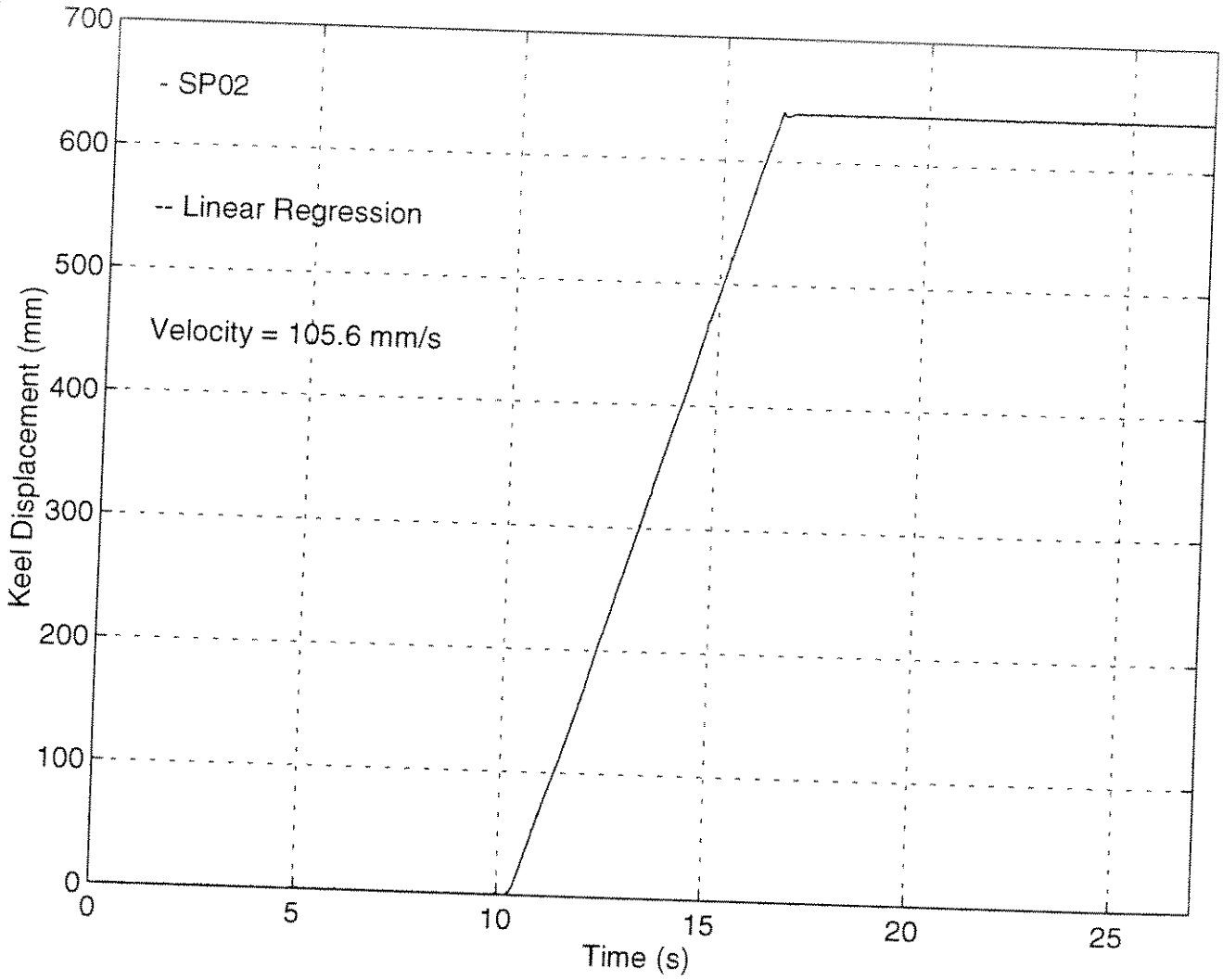

C-CORE

Model Keel Displacement vs. Time for String Potentiometer

Fig. No. 9

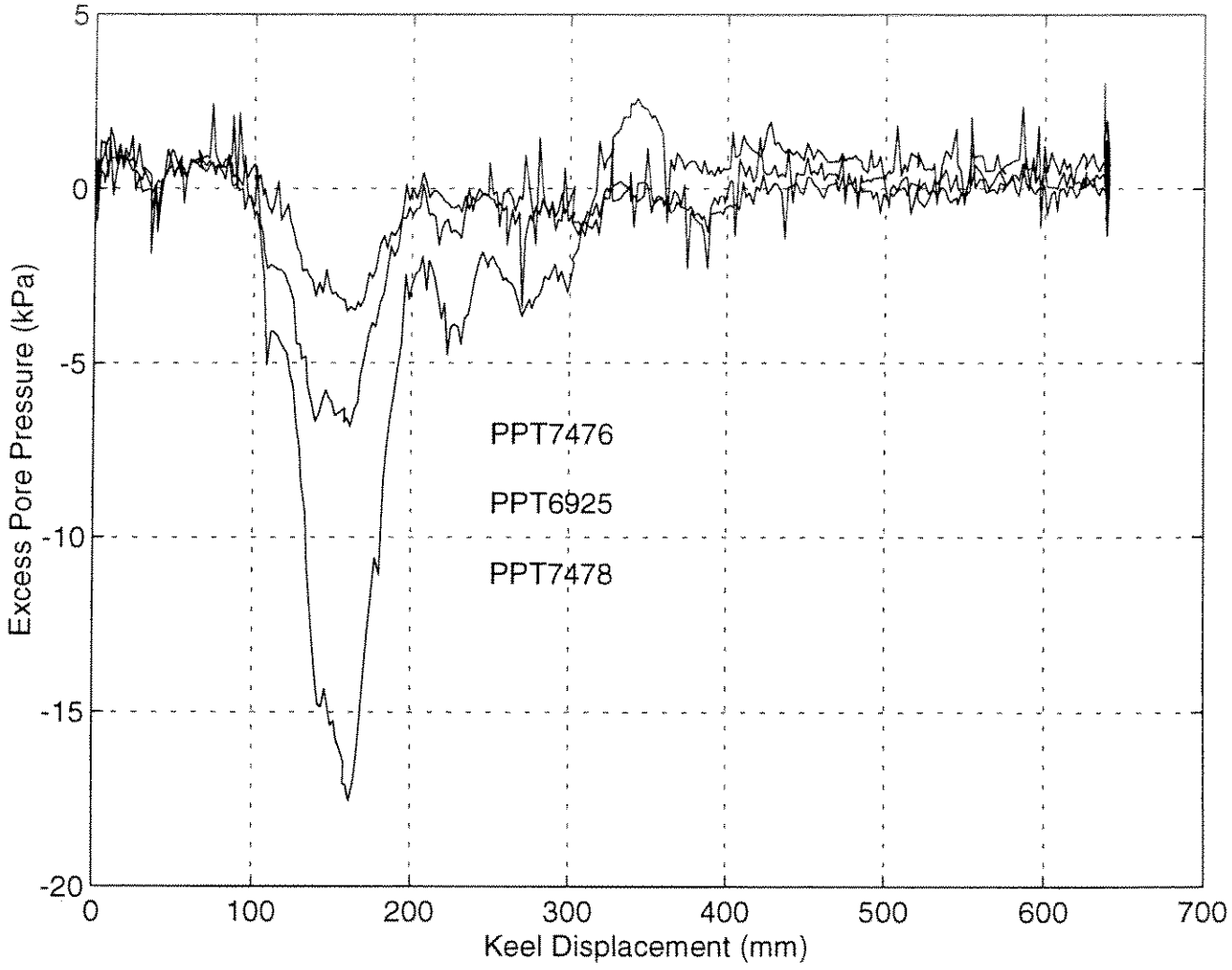

C-CORE

Excess Pore Water Pressure Response during Scour Event

Fig. No. 10

Photographs of Model Scour - Overall Plan and View in Direction of Travel

Fig. No. 11

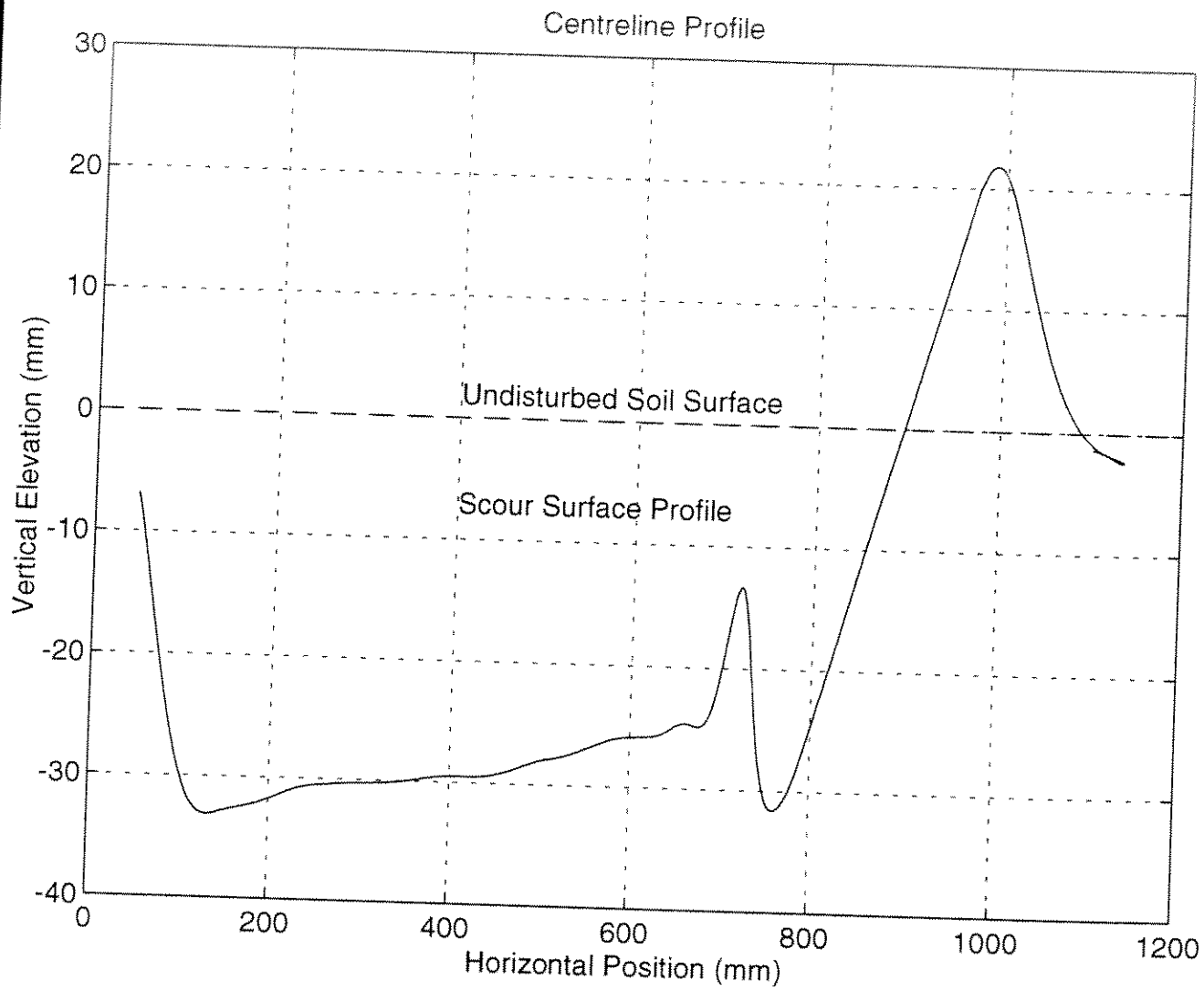

C-CORE

Axial Surface Profile at Scour Centerline

Fig. No. 12

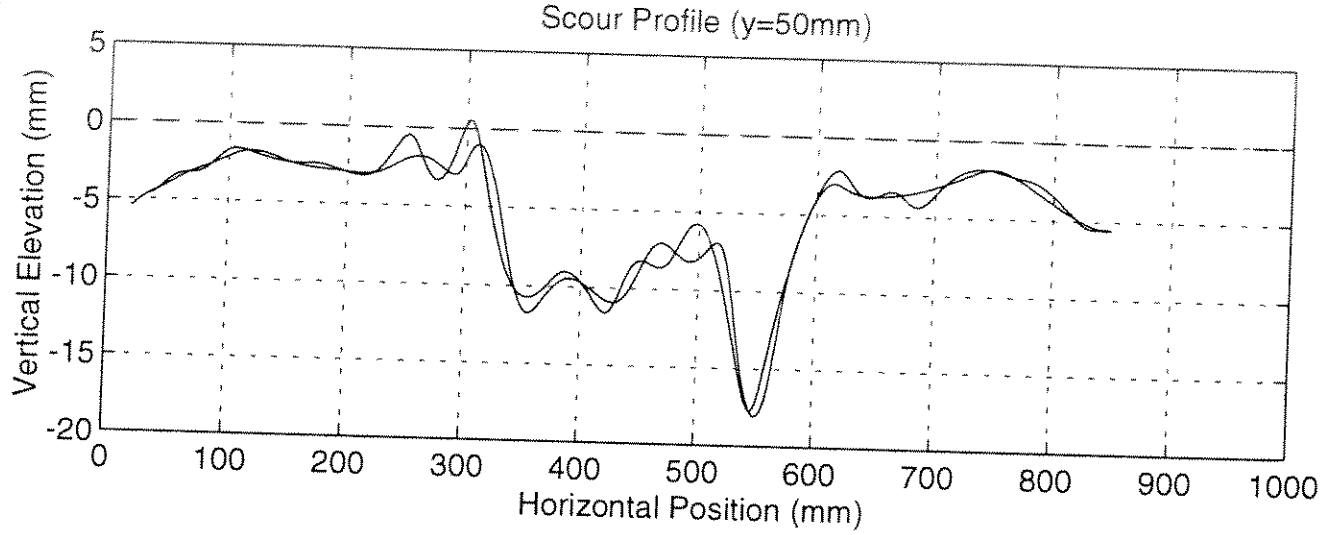

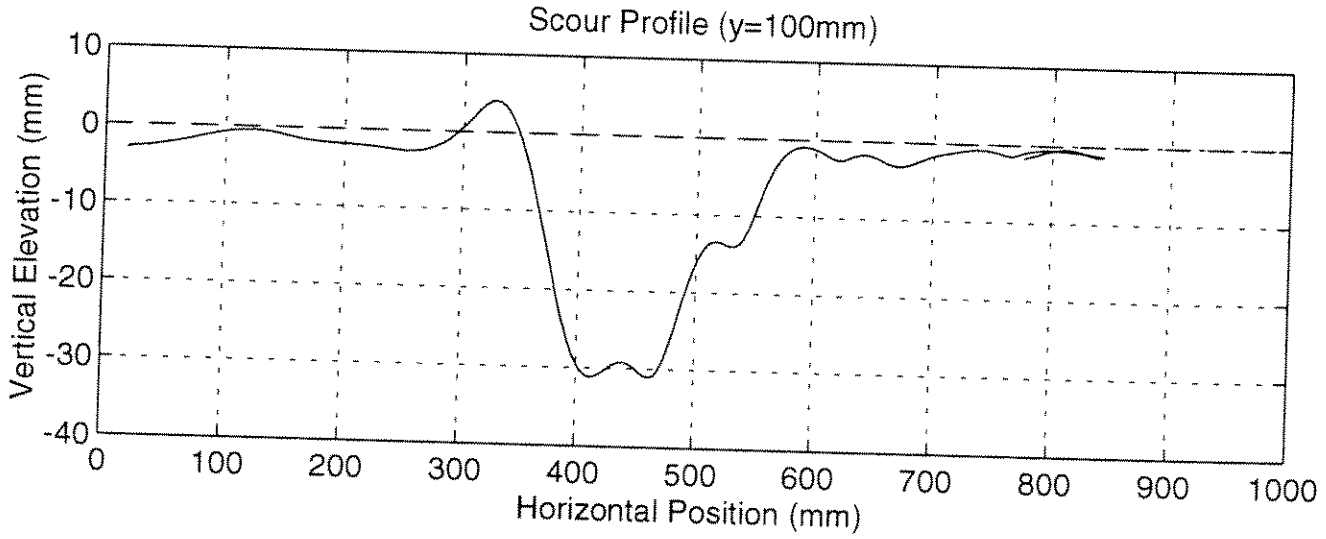

C-CORE

Cross-Sectional Surface Profiles at y=50 mm and 100 mm

Fig. No.

13

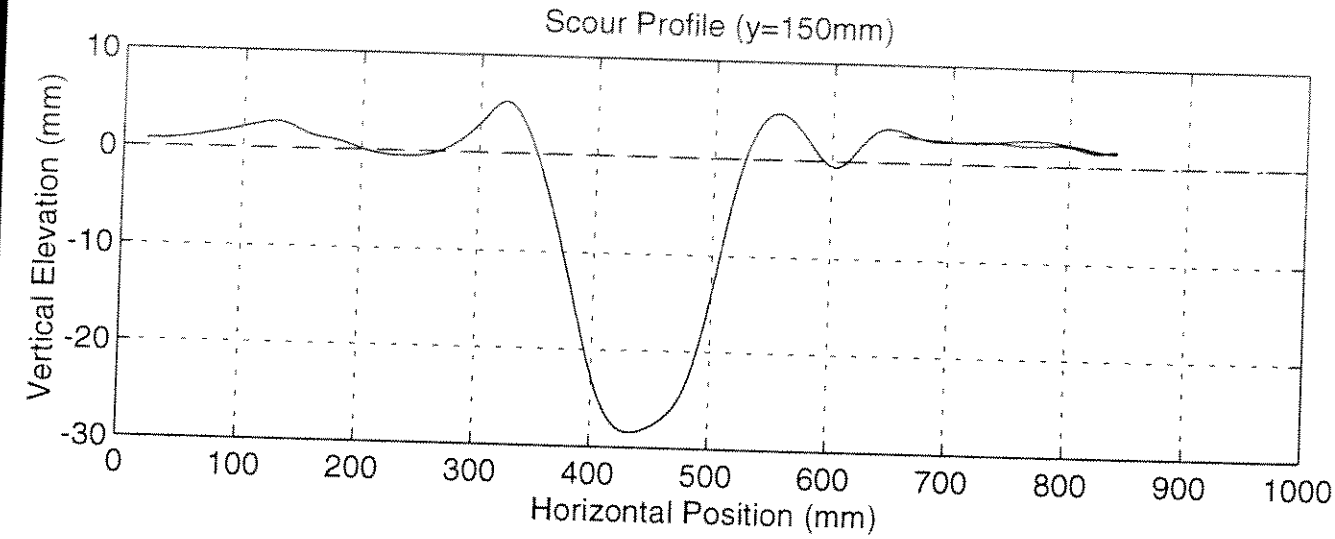

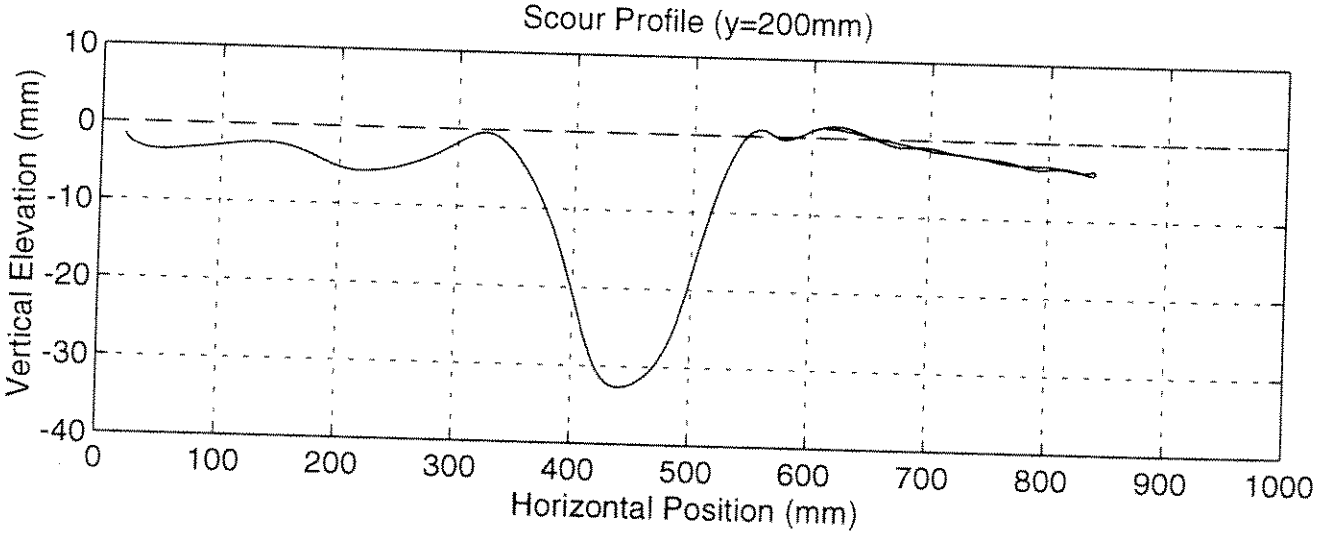

C-CORE

Cross-Sectional Surface Profiles at y=150 mm and 200 mm

Fig. No.

14

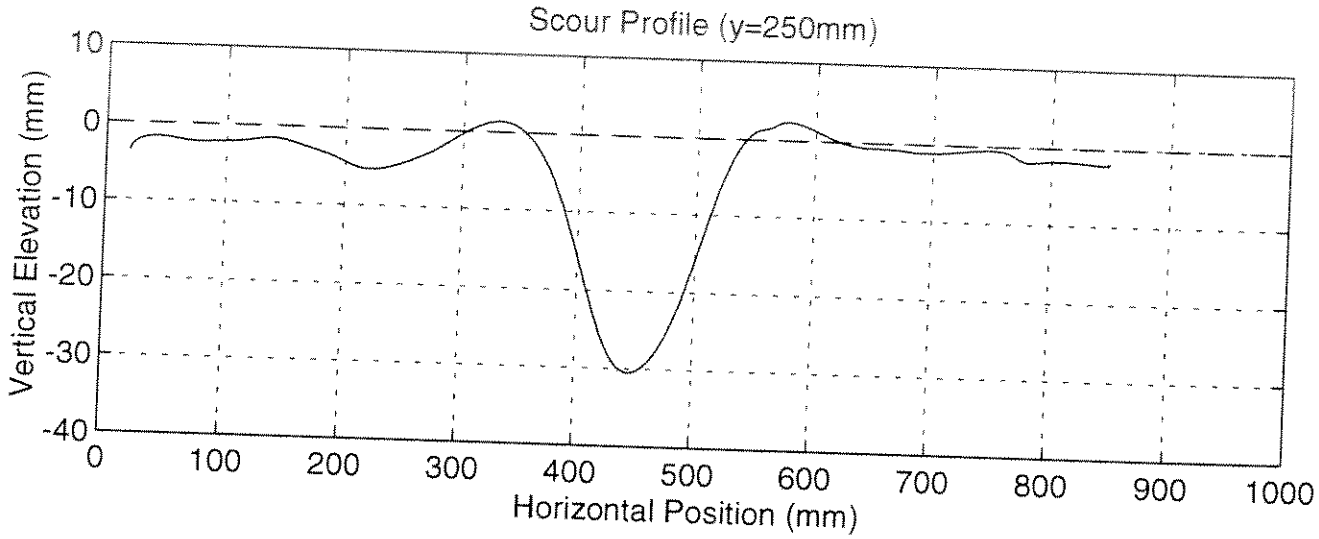

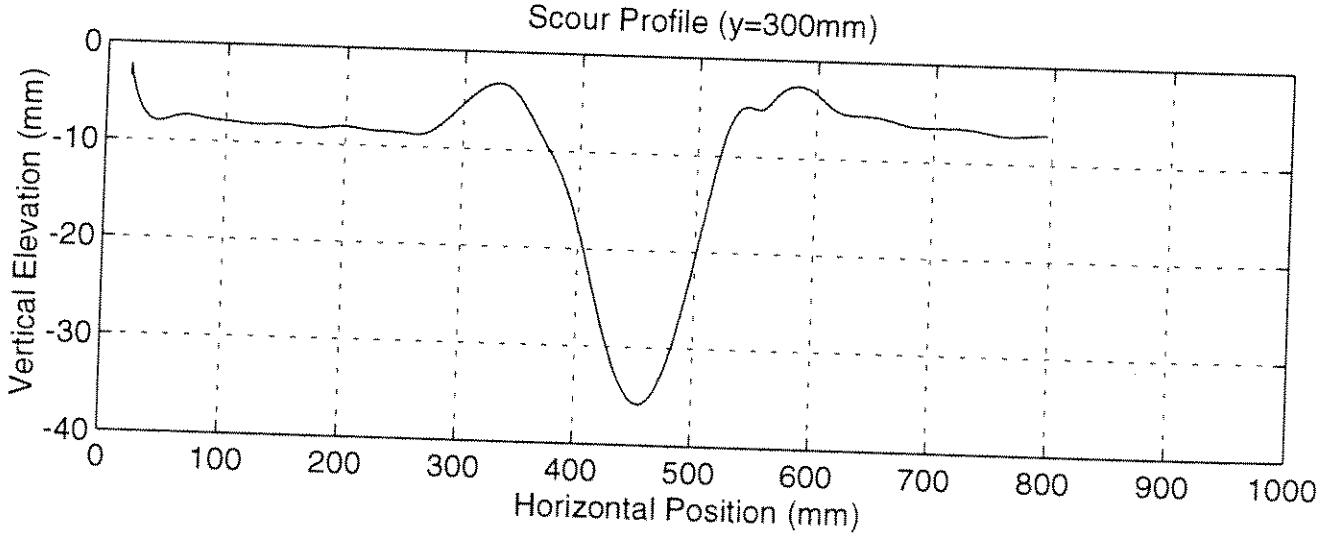

C-CORE

Cross-Sectional Surface Profiles at y=250 mm and 300 mm

Fig. No. 15

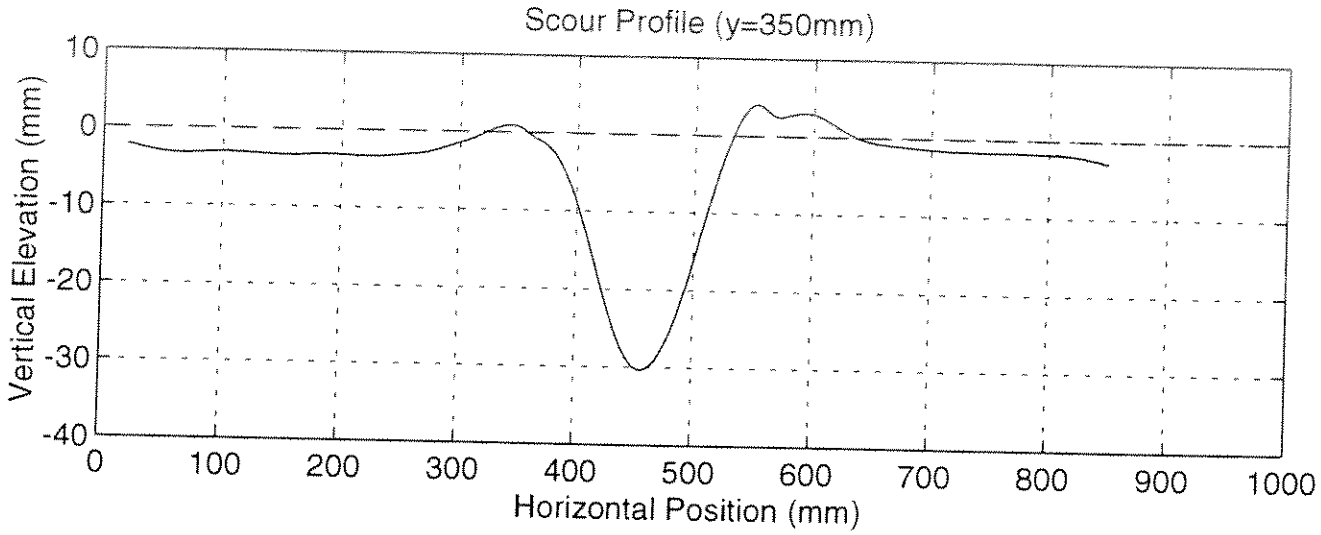

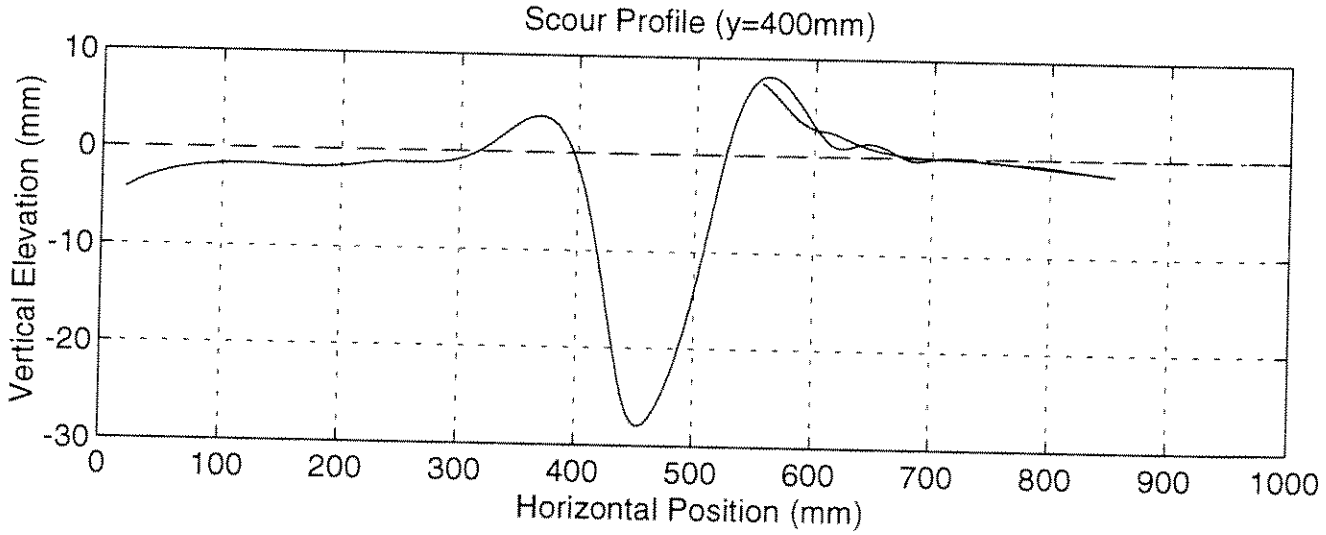

C-CORE

Cross-Sectional Surface Profiles at y=350 mm and 400 mm

Fig. No. 16

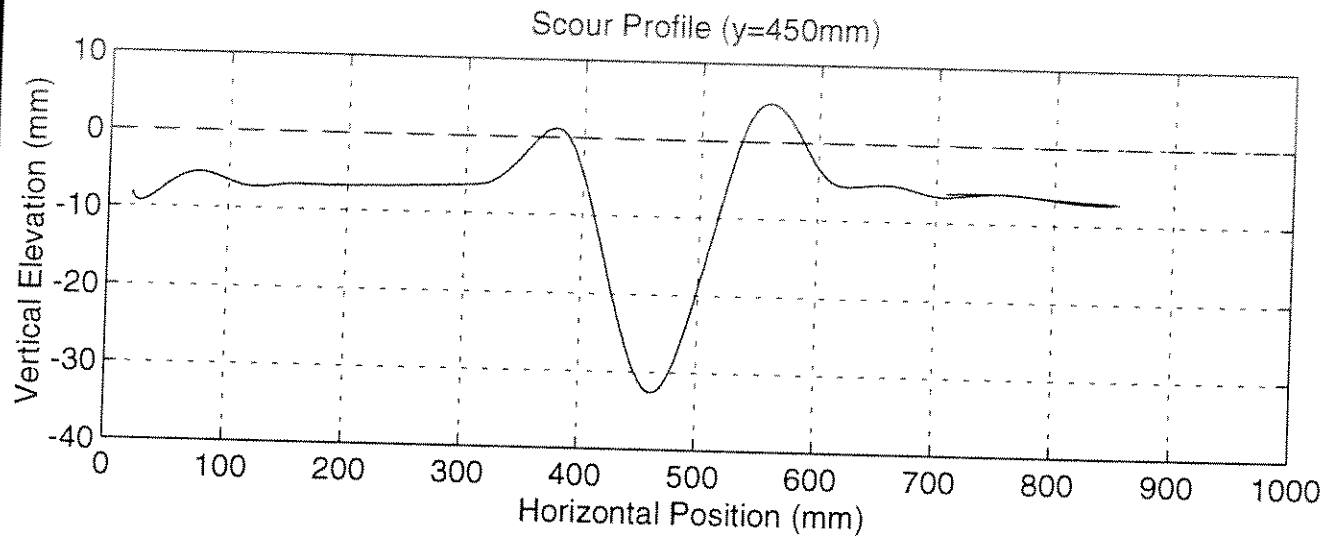

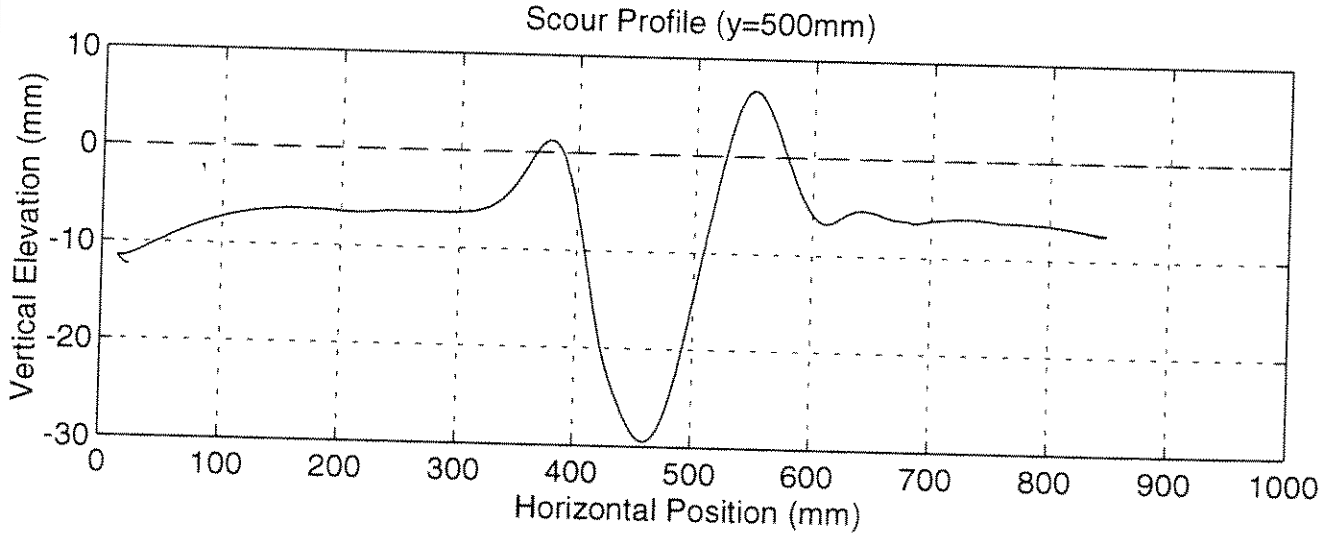

C-CORE

Cross-Sectional Surface Profiles at y=450 mm and 500 mm

Fig. No. 17

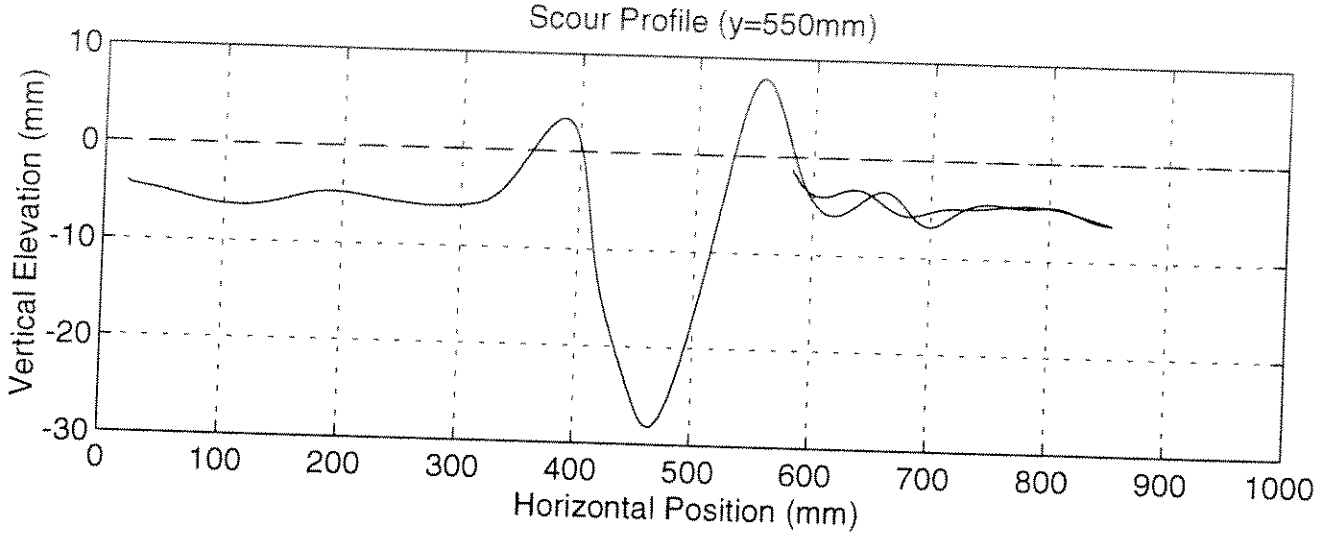

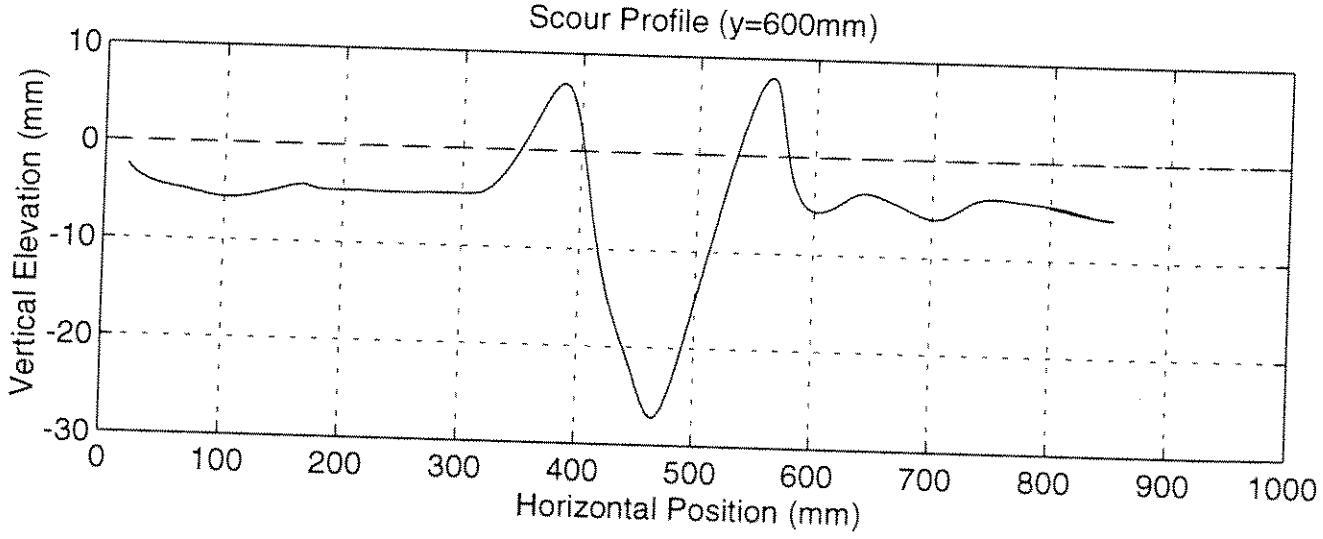

C-CORE

Cross-Sectional Surface Profiles at y=550 mm and 600 mm

Fig. No. 18

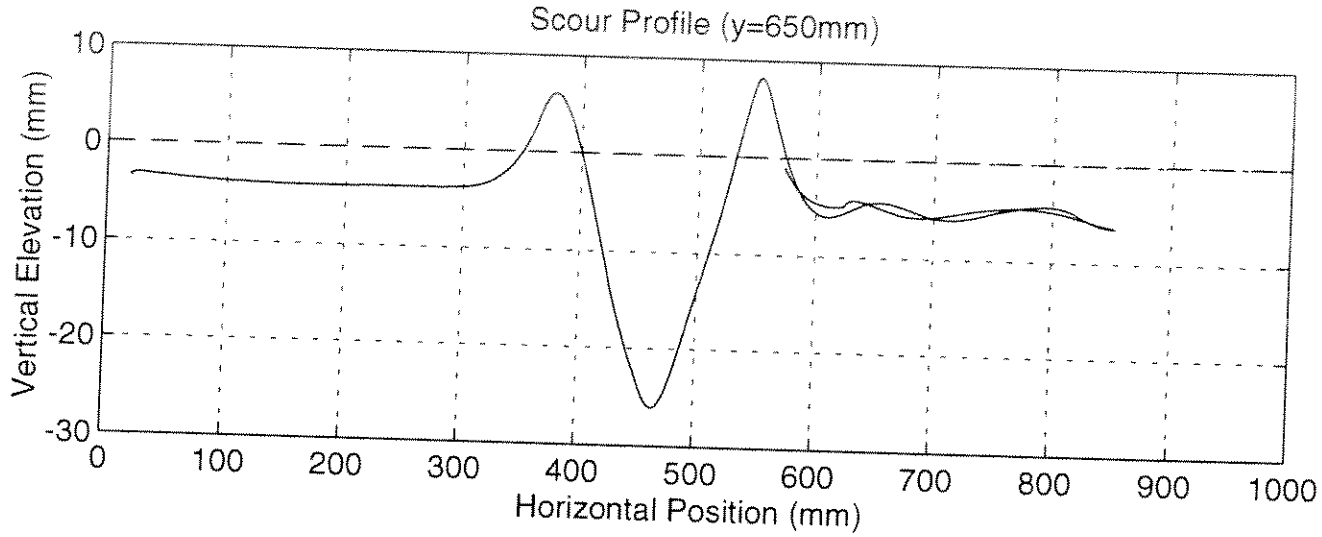

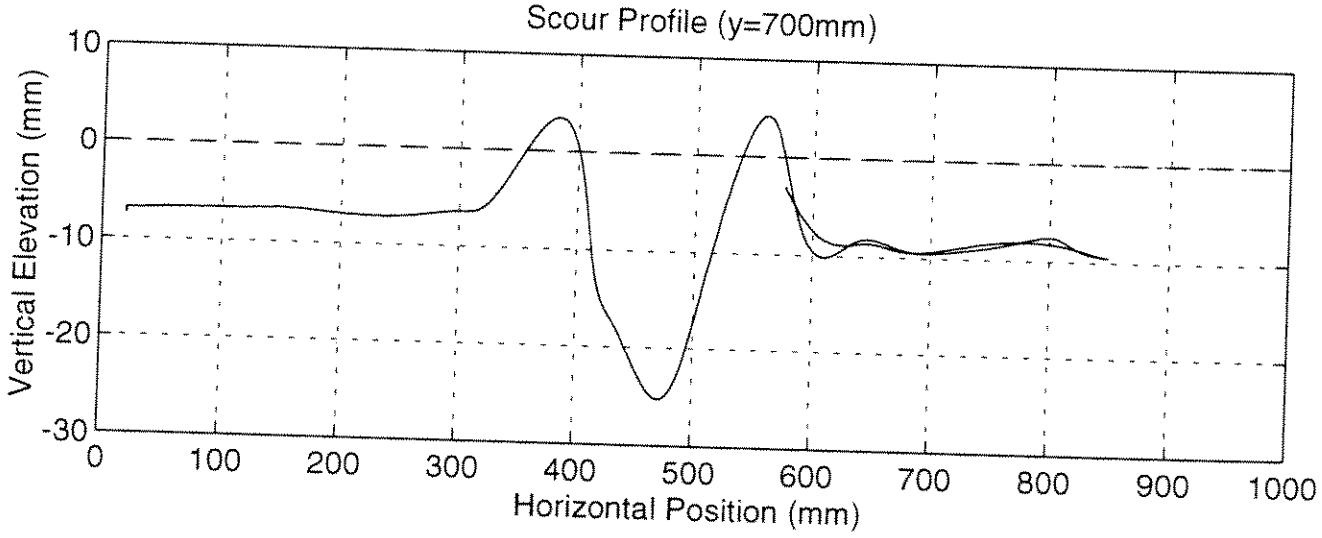

C-CORE

Cross-Sectional Surface Profiles at y=650 mm and 700 mm

Fig. No. 19

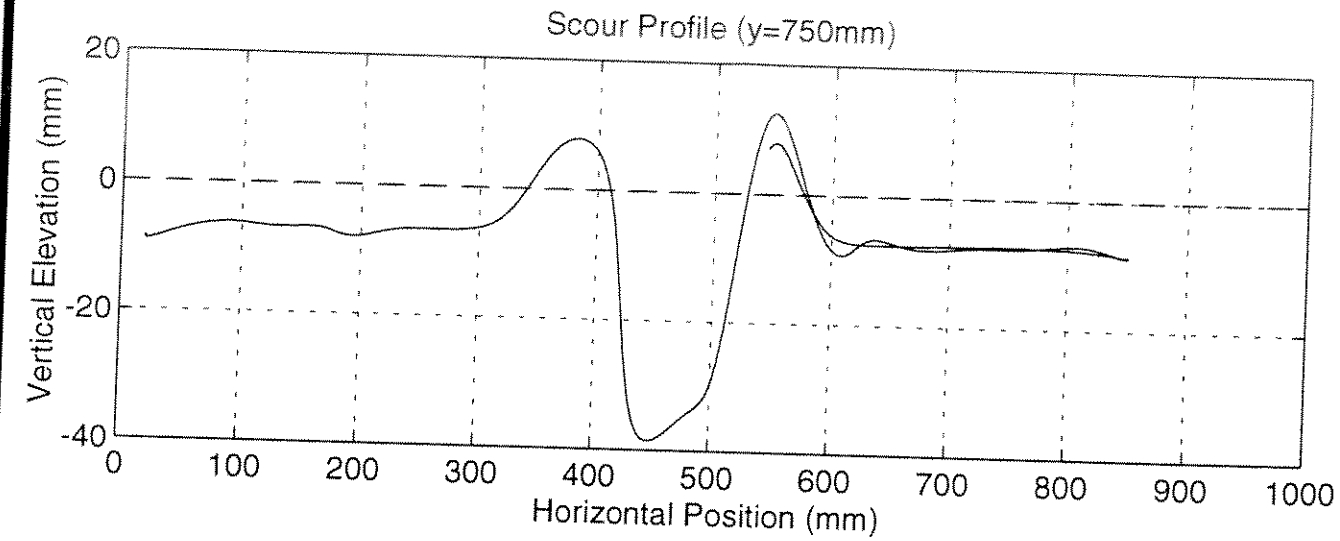

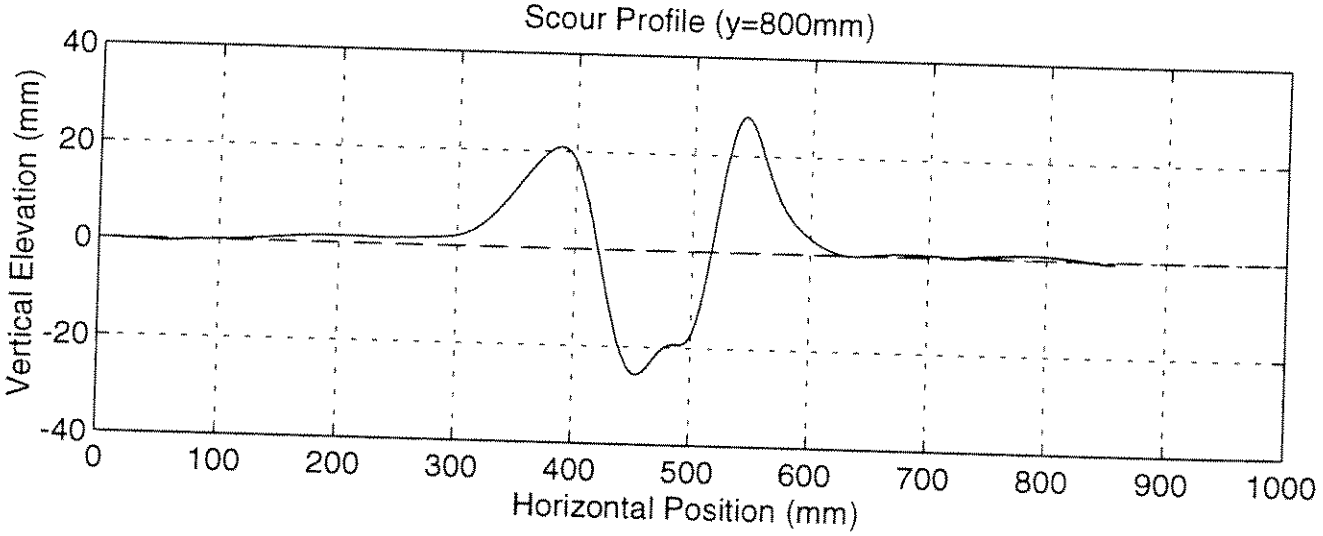

C-CORE

Cross-Sectional Surface Profiles at y=750 mm and 800 mm

Fig. No. 20

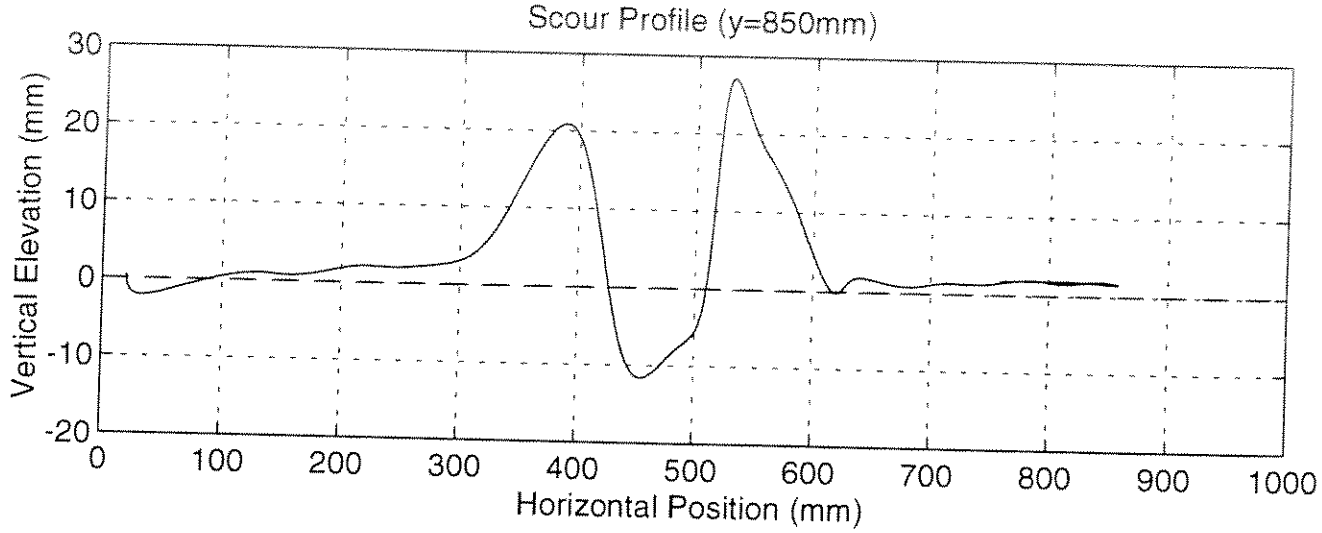

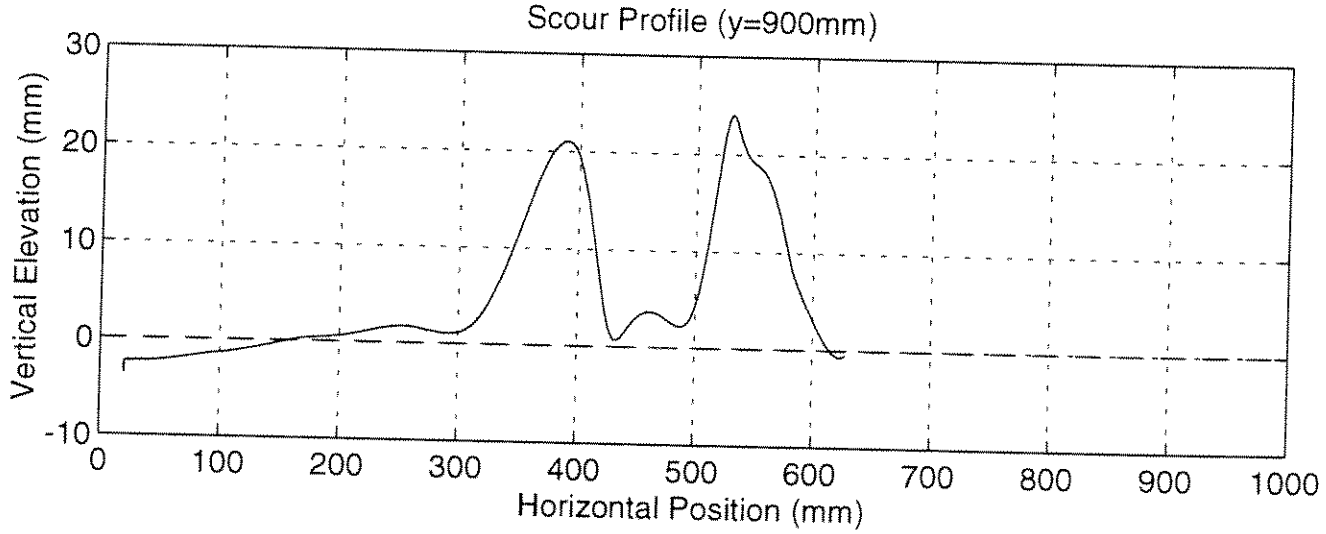

C-CORE

Cross-Sectional Surface Profiles at y=850 mm and 900 mm

Fig. No. 21

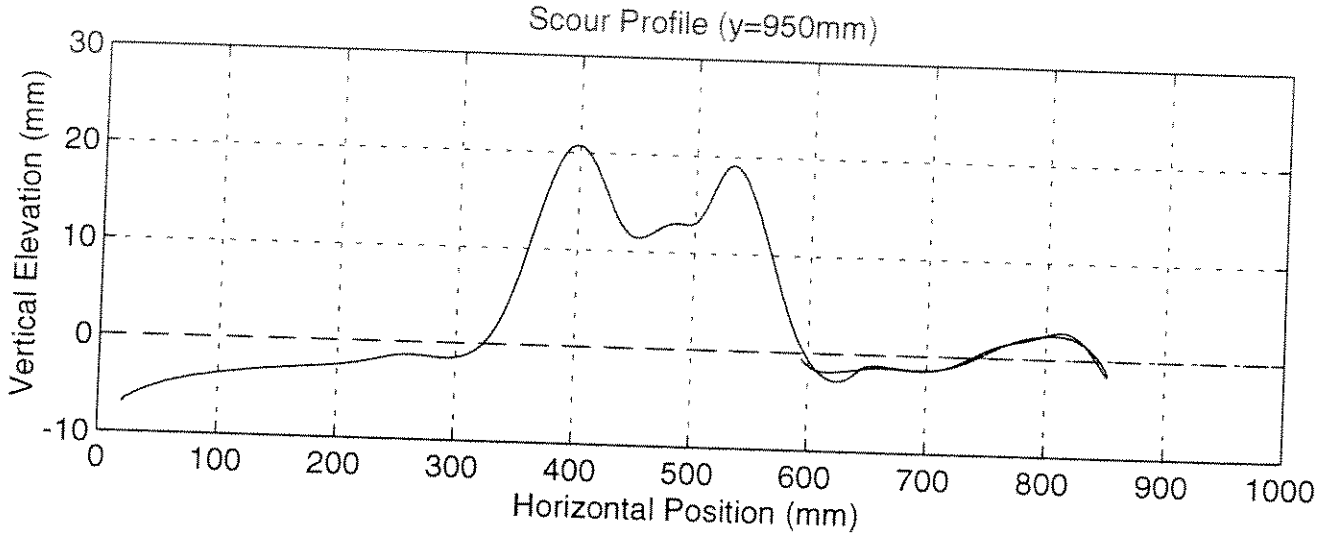

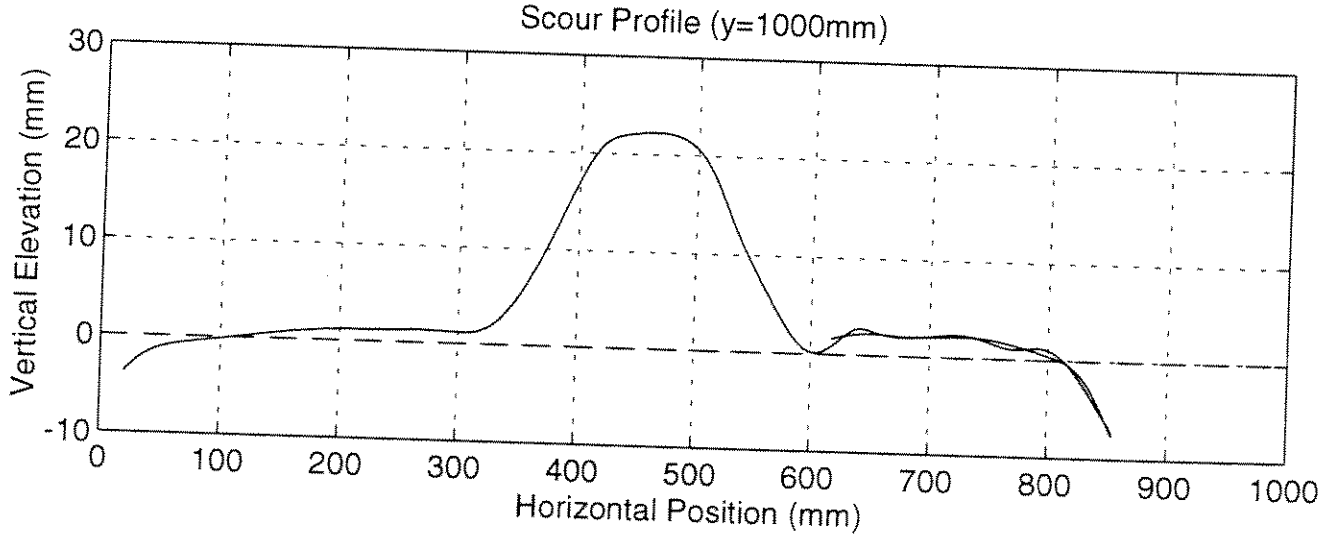

C-CORE

Cross-Sectional Surface Profiles at y=950 mm and 1000 mm

Fig. No. 22

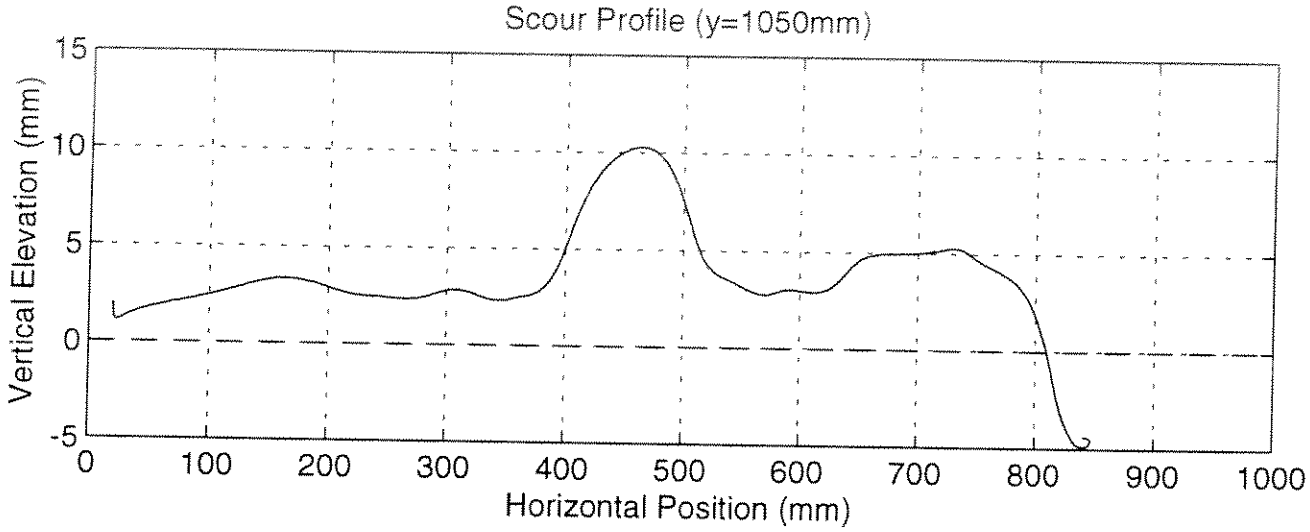

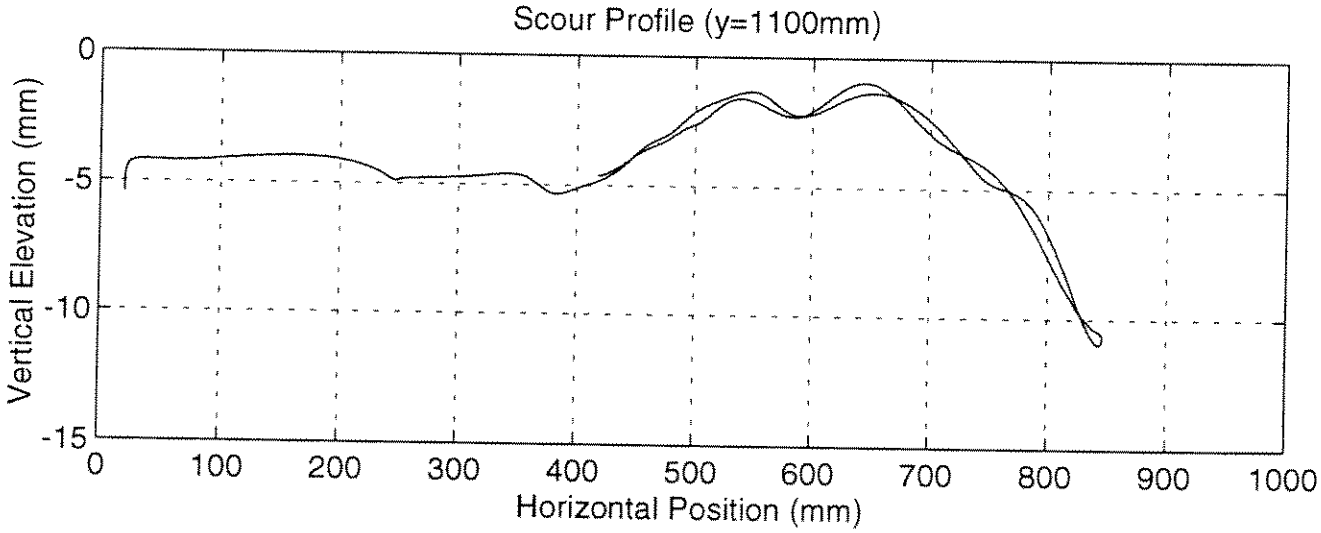

C-CORE

Cross-Sectional Surface Profiles at y=1050 mm and 1100 mm

Fig. No. 23

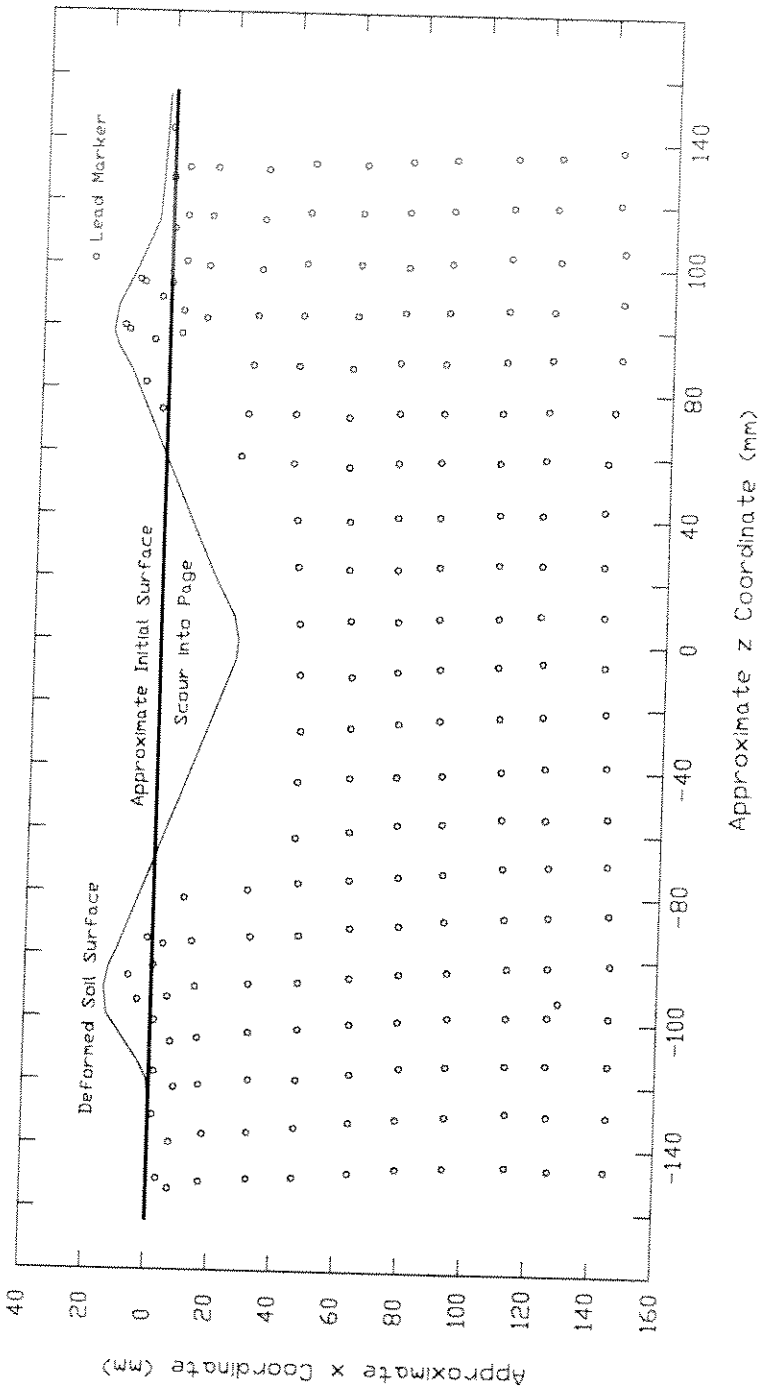

C-CORE

Trace of Cross Section Radiograph Showing Lateral Marker Grid at y=540 mm

Fig. No.

24

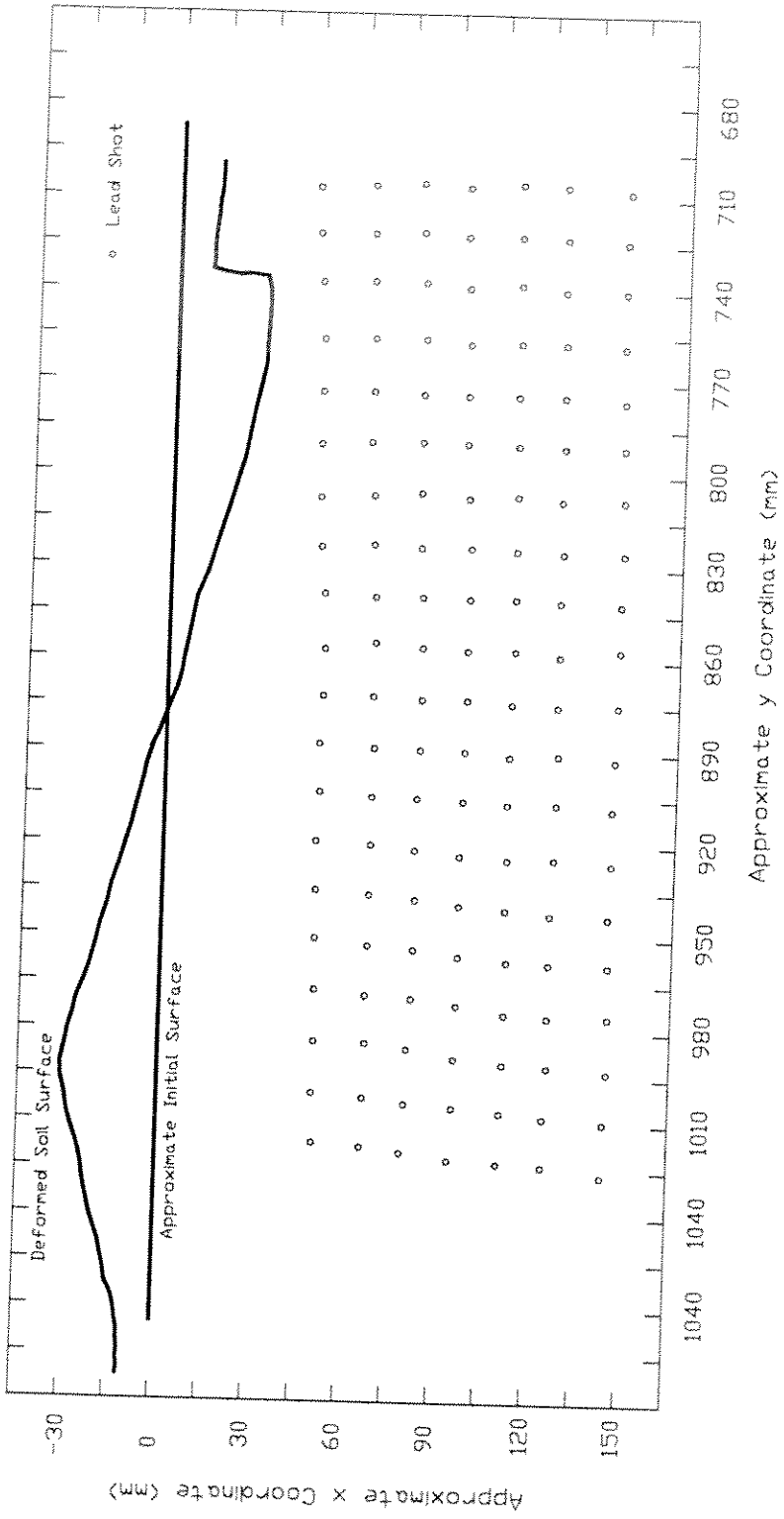

C-CORE

Trace of Axial Section Radiograph Showing Centerline Marker Grid at Final Model Position

Fig. No.

25

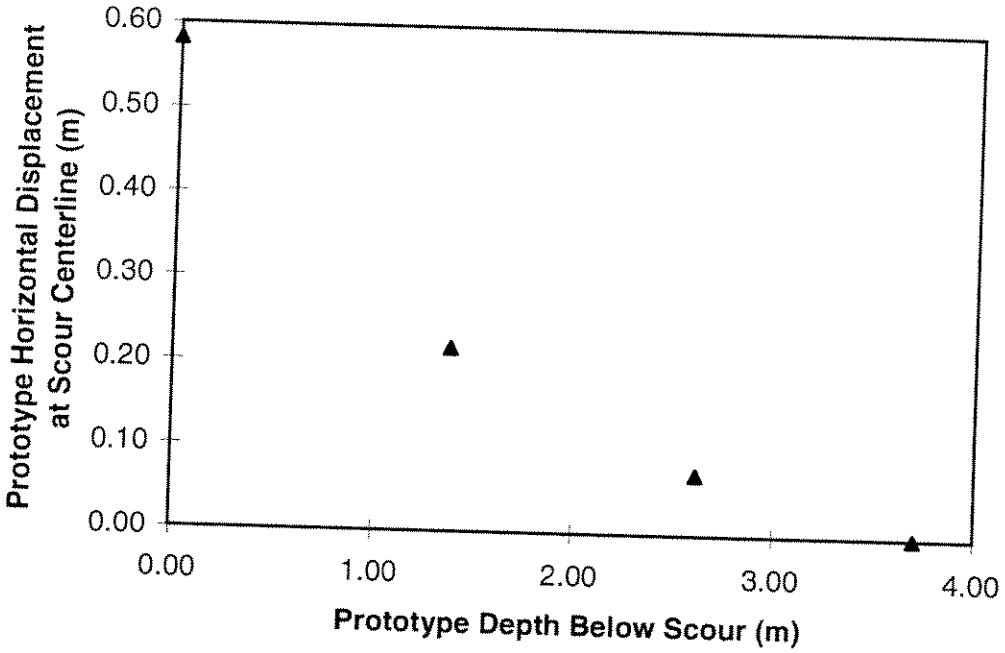

C-CORE

Average Centerline Values of Horizontal Soil Displacement vs. Depth Below Scour Base

Fig. No. 26

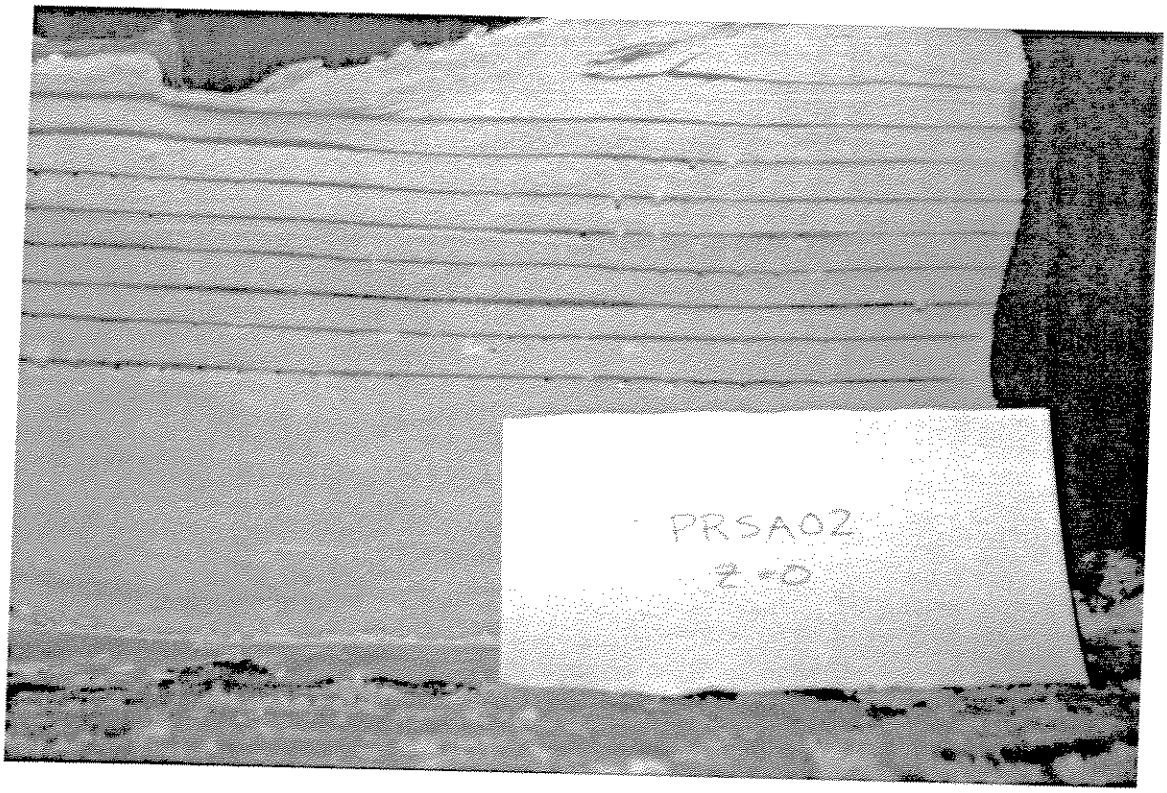

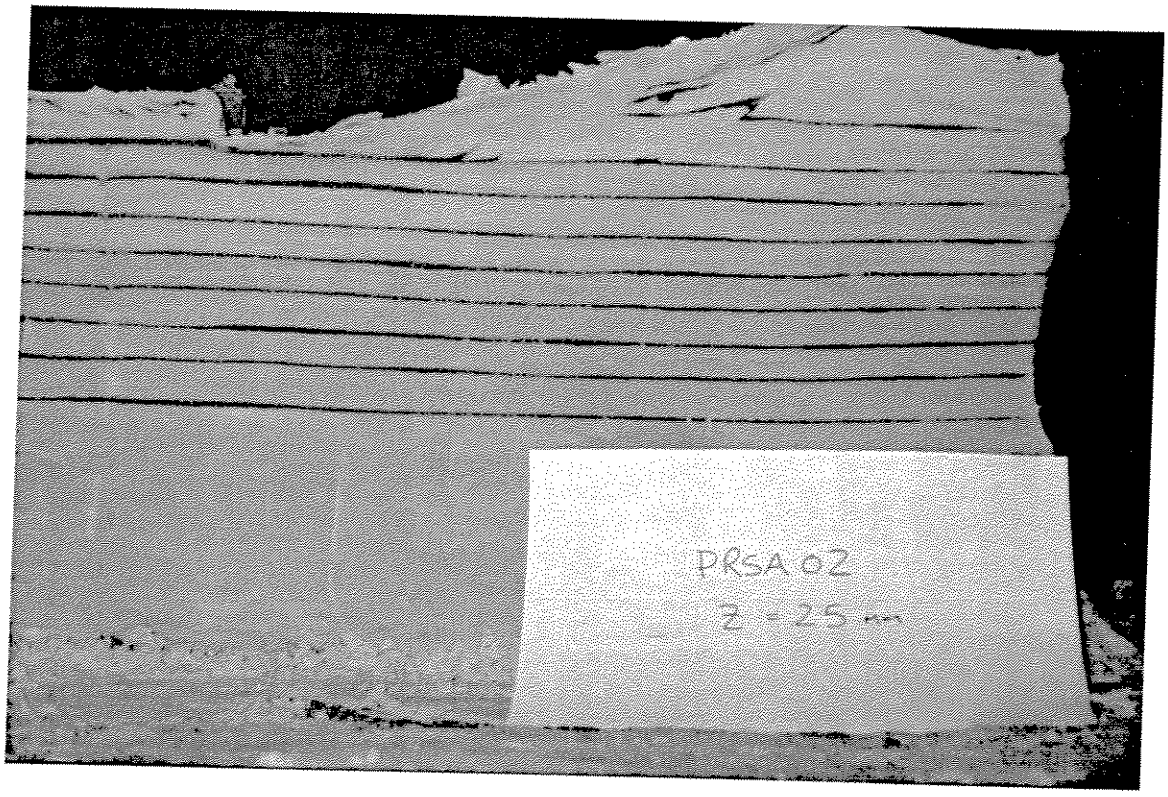

C-CORE

Photographs of Axial Testbed Sections beneath Keel at Final Position, y = 700 to 1010mm, z = 0 and 25mm

Fig. No. 27

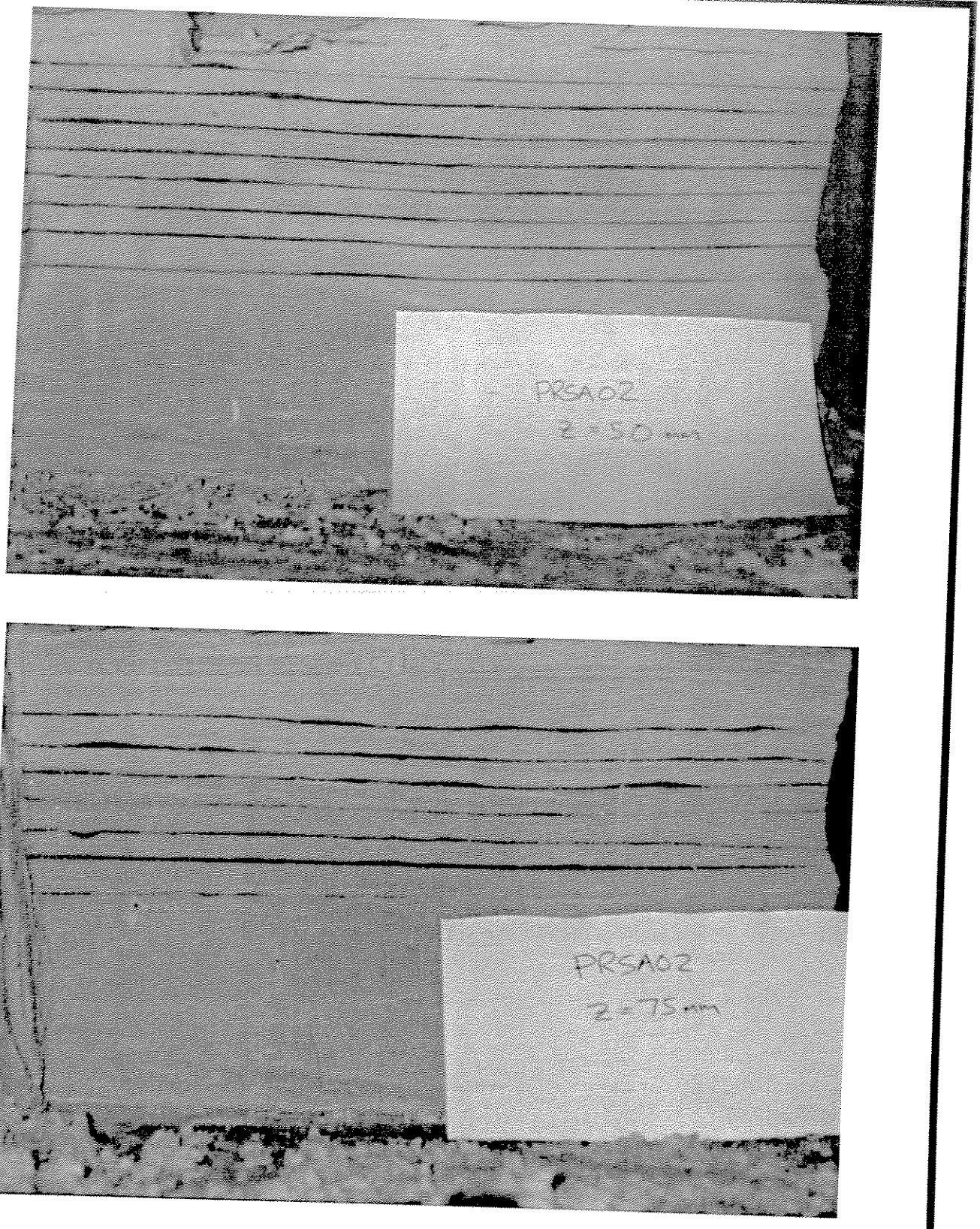

C-CORE

Photographs of Axial Testbed Sections beneath Keel at Final Position, y = 700 to 1010mm, z = 50 and 75mm

Fig. No. 28

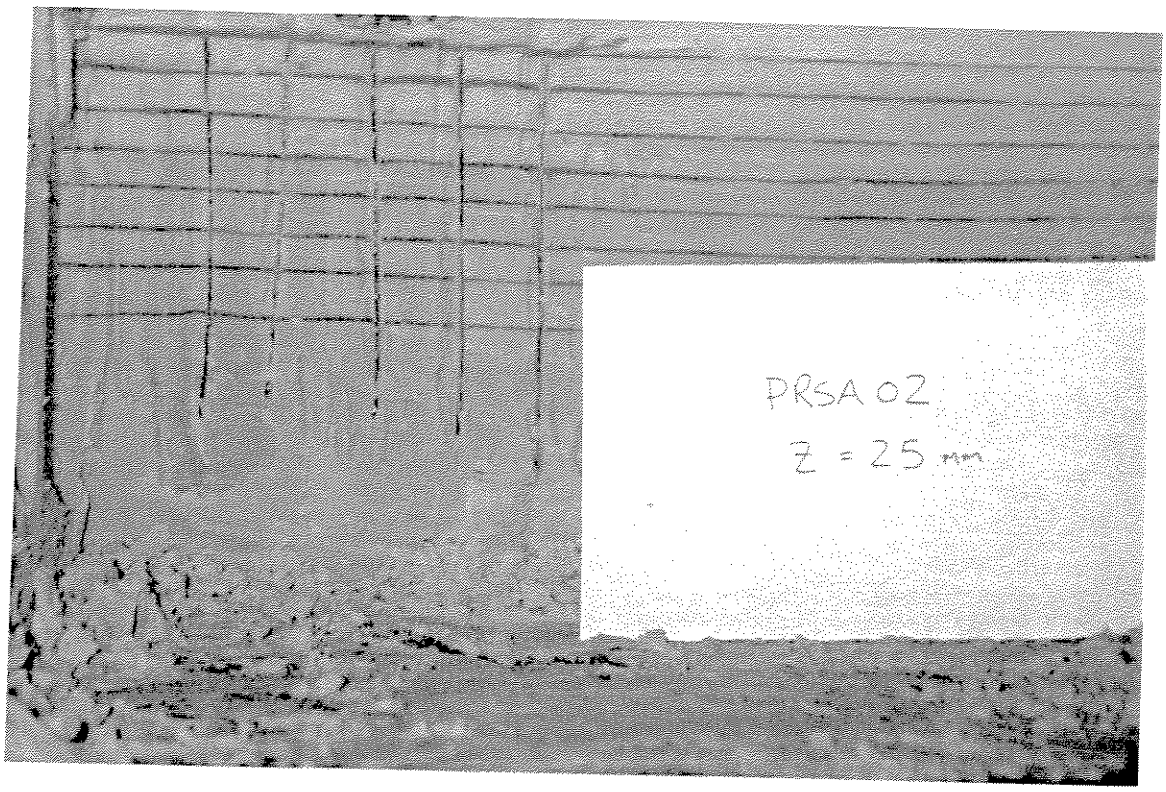

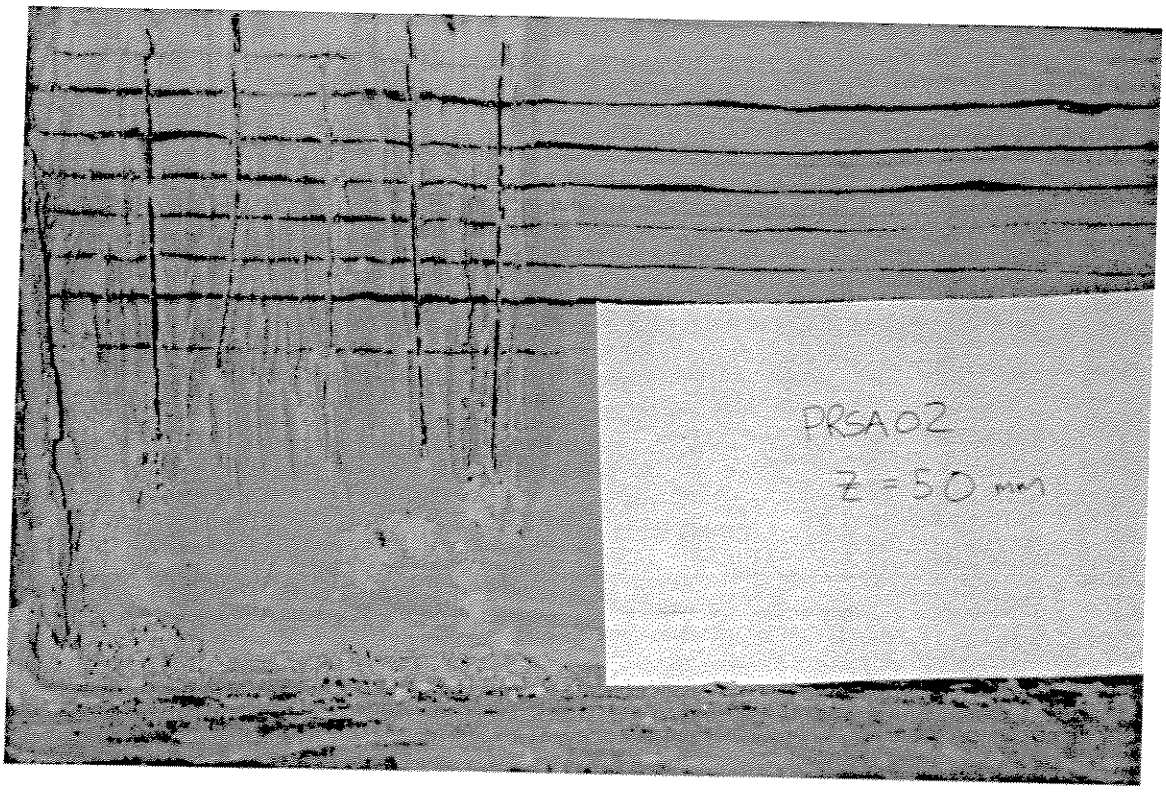

C-CORE

Photographs of Axial Testbed Sections beneath Keel at Final Position, y = 700 to 1010mm, z = 25 and 50mm

Fig. No.

29

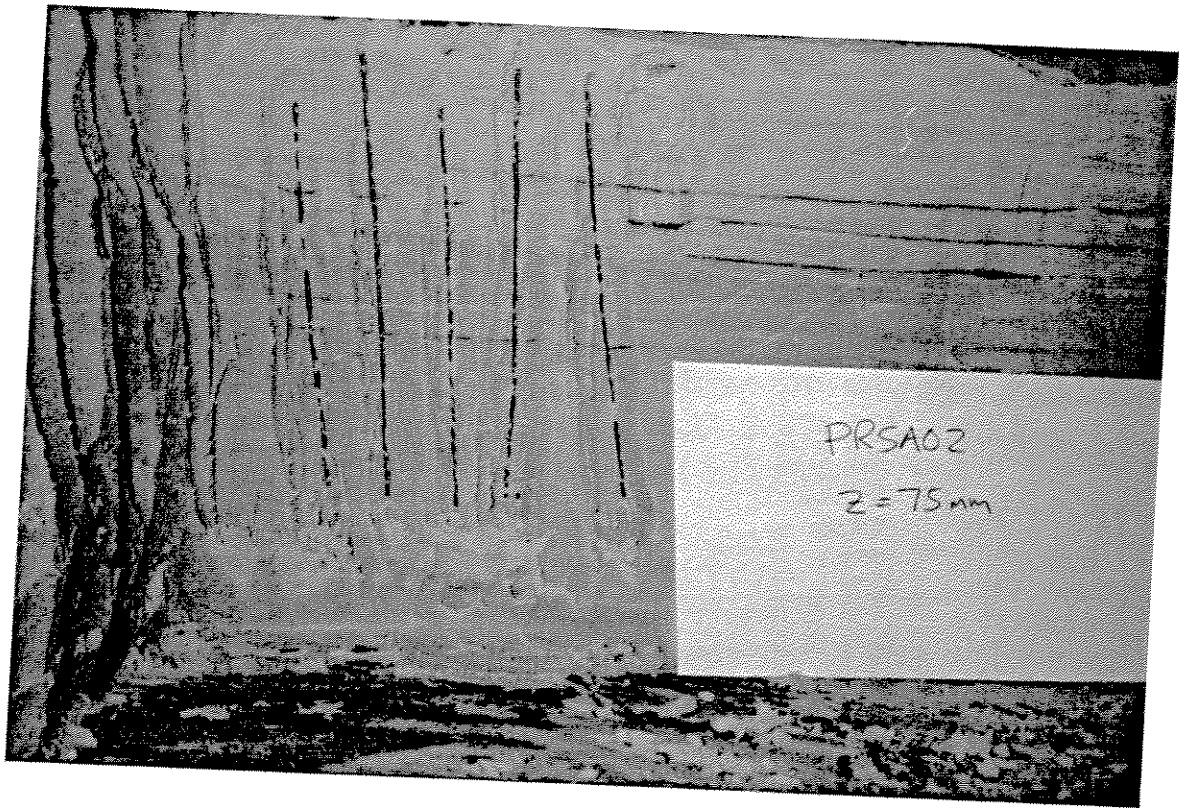

C-CORE

Photograph of Axial Testbed Section beneath Keel at Final Position, y = 700 to 1010mm, z = 75mm

Fig. No.

30

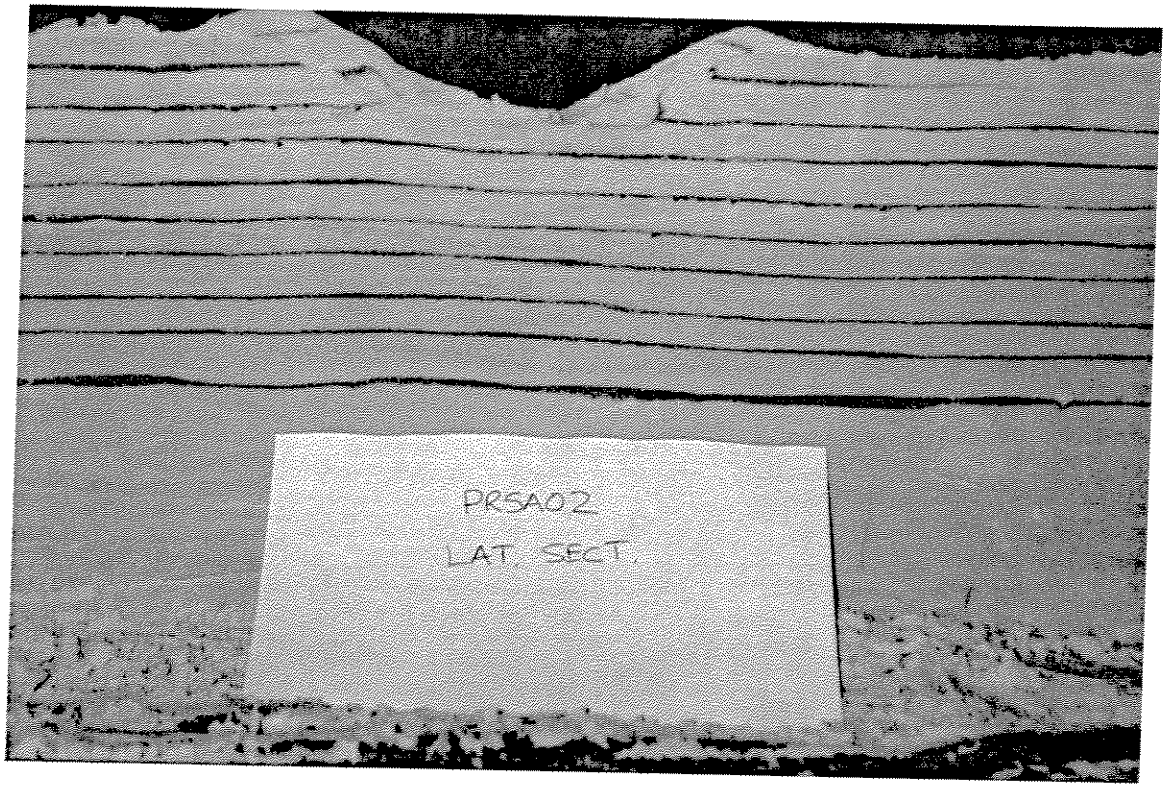

C-CORE

Photograph of Lateral Testbed Section on Scour Centerline, y = 540mm, z = -150 to 150mm

Fig. No.

31